This copy is for personal use only. To order printed copies, contact *reprints@rsna.org*

Traumatic Brain Injury: Imaging Patterns and Complications

Andrew D. Schweitzer, MD
Sumit N. Niogi, MD, PhD
Christopher J. Whitlow, MD, PhD, MHA
A. John Tsiouris, MD

Abbreviations: ACR = American College of Radiology, CSF = cerebrospinal fluid, DAI = diffuse axonal injury, DTI = diffusion-tensor imaging, EDH = epidural hematoma, FLAIR = fluid-attenuated inversion recovery, GCS = Glasgow Coma Scale, SAH = subarachnoid hemorrhage, SDH = subdural hematoma, TAI = traumatic axonal injury, TBI = traumatic brain injury, 3D = three dimensional

RadioGraphics 2019; 39:1571–1595

https://doi.org/10.1148/rg.2019190076

Content Codes: CT ER HN MR NR

From the Department of Radiology, Weill Cornell Medicine/New York–Presbyterian Hospital, 525 E 68th St, Starr 630C, New York, NY 10075 (A.D.S., S.N.N., A.J.T.); and Department of Radiology, Wake Forest School of Medicine, Winston-Salem, N.C. (C.T.W.) Received March 22, 2019; revision requested May 31 and received June 15; accepted June 19. For this journal-based SA-CME activity, the authors S.N.N. and A.J.T. have provided disclosures (see end of article); all other authors, the editor, and the reviewers have disclosed no relevant relationships. **Address correspondence to** A.J.T. (e-mail: *apt9001@med.cornell.edu*).

See discussion on this article by Mathur and Nicolaou (pp 1595–1597).

©RSNA, 2019

SA-CME LEARNING OBJECTIVES

After completing this journal-based SA-CME activity, participants will be able to:

- Understand the benefits and limitations of CT, MRI, and angiographic techniques in TBI.
- Describe the primary injury patterns of TBI on the basis of the mechanism of injury.
- Recognize secondary injuries that can occur as complications of mass effect and herniation.

See rsna.org/learning-center-rg.

While the diagnosis of traumatic brain injury (TBI) is a clinical decision, neuroimaging remains vital for guiding management on the basis of identification of intracranial pathologic conditions. CT is the mainstay of imaging of acute TBI for both initial triage and follow-up, as it is fast and accurate in detecting both primary and secondary injuries that require neurosurgical intervention. MRI is more sensitive for the detection of certain intracranial injuries (eg, axonal injuries) and blood products 24–48 hours after injury, but it has limitations (eg, speed, accessibility, sensitivity to motion, and cost). The evidence primarily supports the use of MRI when CT findings are normal and there are persistent unexplained neurologic findings or at subacute and chronic periods. Radiologists should understand the role and optimal imaging modality to use, in addition to patterns of primary brain injury and their influence on the risk of developing secondary brain injuries related to herniation.

©RSNA, 2019 • *radiographics.rsna.org*

Introduction

Traumatic brain injury (TBI) is a major public health problem, with an estimated yearly global incidence of 69 million and with an increasing prevalence over the past 25 years (1,2). In the United States in 2013, there were nearly 2.8 million TBI diagnoses, 282 000 TBI-related hospitalizations, and 56 000 TBI-related deaths (3). Imaging—CT and, to an increasing extent, MRI—plays a critical role in TBI management and prognostication (4). This article reviews the classifications of TBI, summarizes the utility of each imaging modality, and presents TBI imaging findings categorized by anatomic location. Illustrative cases highlight important injury patterns and their mechanisms, and findings that influence management and prognosis are emphasized.

Classification of TBI

Glasgow Coma Scale

TBI is a clinical diagnosis traditionally classified using the Glasgow Coma Scale (GCS). GCS scores 13–15 are mild brain injuries, 9–12 are moderate, and 3–8 are severe. There is a strong correlation between GCS score and morbidity and/or mortality at the severe end of the spectrum but limited correlation at the mild end of the spectrum.

The GCS has been a long-standing clinical tool used to quickly categorize TBI as mild, moderate, or severe solely on the basis of physical examination findings without the need to use specialized tools. GCS score is determined by summing the scores from three categories: best eye response (score 1–4), best verbal response (score 1–5), and best motor response (score 1–6), yielding scores of 3–8 (severe), 9–12 (moderate), and 13–15 (mild) (5). The value of this method has been

TEACHING POINTS

- TBI is a clinical diagnosis traditionally classified using the GCS. GCS scores 13–15 are mild brain injuries, 9–12 are moderate, and 3–8 are severe. There is a strong correlation between GCS score and morbidity and/or mortality at the severe end of the spectrum but limited correlation at the mild end of the spectrum.
- Nonenhanced head CT is critical for triage, imaging of intracranial pathologic conditions, and follow-up of patients with intracranial findings given its speed, accessibility, and sensitivity for depicting brain injuries that require neurosurgical intervention, such as large-volume hemorrhage, herniation, and infarction
- MRI has substantially higher sensitivity than CT for the detection of EDH, SDH, nonhemorrhagic cortical contusions, brainstem injuries, and white matter axonal injuries (supported by level Ib evidence).
- It is important to note that mixed-attenuation SDHs are not necessarily acute on chronic. The hypoattenuating portions may represent hyperacute and/or unclotted chronic blood products, particularly in patients with coagulopathy.
- DAI can be hemorrhagic and/or nonhemorrhagic, and both hemorrhagic and nonhemorrhagic lesions are more sensitively detected at MRI. Acute DAI lesions may restrict diffusion. Characteristic locations for TAI lesions include the gray-white matter junction (especially in the frontal lobes because the axis of rotation of the head is posterior, allowing greater differences in momentum anteriorly), corpus callosum (especially the splenium), internal capsules, and dorsal midbrain and/or pons.

its ease of use combined with the strong correlation to morbidity and mortality at the severe end of the TBI spectrum.

The GCS still remains a primary tool both clinically and in research for the classification of TBI. Unfortunately, correlation with morbidity on the mild end of the spectrum is poor. A perfect score of 15 does not signify absence of a TBI, nor does it exclude the possible development of postconcussive syndrome. Despite the gross limitations for patients with mild TBI, a recent review of 811 143 patients from the National Trauma Data Bank showed that a GCS score less than or equal to 13 can discriminate the need for trauma center care (6). GCS scores have been used to discriminate in-hospital mortality, receipt of neurosurgical interventions, severe brain injury, and emergency intubation (7). For mild TBI, duration of loss of consciousness and posttraumatic amnesia have a much stronger correlation with outcome and worse Glasgow Outcome Scale scores at 6–12 months (8).

American Academy of Neurology Concussion Guidelines

The terms *TBI* and *concussion* historically have often been used interchangeably. In recent years, concussion has been more closely linked to mild TBI. Moreover, recent efforts have focused on further refinement of these definitions. Concussion has been suggested to reflect a transient condition avoiding the potential stigma associated with brain injury (9).

Along these efforts, in 2013 the American Academy of Neurology revised the prior 1997 concussion guidelines (10). These new guidelines report that concussion is a clinical diagnosis and that CT "should not be used to diagnose sports-related concussion but might be obtained to rule out more serious TBI such as an intracranial hemorrhage in athletes with a suspected concussion who have LOC [loss of consciousness], posttraumatic amnesia, persistently altered mental status ([GCS] <15), focal neurologic deficit, evidence of skull fracture on examination, or signs of clinical deterioration (Level C evidence)" (10).

Imaging Utilization

Nonenhanced head CT is critical for triage, imaging of intracranial pathologic conditions, and follow-up of patients with intracranial findings given its speed, accessibility, and sensitivity for depicting brain injuries that require neurosurgical intervention, such as large- volume hemorrhage, herniation, and infarction. Other specific benefits of CT over MRI include a much higher sensitivity for the detection of a fracture (associated with epidural hematoma [EDH], vascular injury, and cerebrospinal fluid [CSF] leak) and no need to screen for safety, which is especially important in penetrating or blast injuries (Figs 1–5). The New Orleans Criteria, the Canadian Head CT Rule, and the National Emergency X-Radiography Utilization Study II (NEXUS-II) criteria are the most widely used clinical decision-making tools that help determine whether nonenhanced head CT is clinically warranted in cases of mild TBI (11). These criteria are used to inform the American College of Radiology (ACR) Appropriateness Criteria for head trauma (12–14). Nonenhanced head CT is a class I recommendation for patients with moderate to severe TBI (4).

For the nonenhanced CT protocol for adults, we recommend using multidetector CT, axial views, head tilt or angled gantry to reduce lens radiation exposure, 120 kVp, 240 mAs, 22-cm field of view, and 5-mm section thickness. The following reconstructions should be obtained: *(a)* axial images at 2.5-mm sections in standard algorithm, *(b)* axial images at 5-mm sections in standard algorithm, *(c)* axial images at 2.5-mm sections in bone algorithm, *(d)* coronal images at 2 × 2-mm sections, *(e)* sagittal images at 2 × 2-mm sections, and *(f)* axial images at 0.625-mm sections that can be used to make 3D reconstructions of

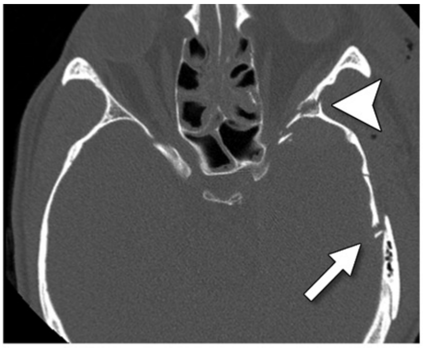

Figure 1. Blunt head injury with depressed skull fracture, complex maxillofacial fractures, venous and arterial EDH, subdural hematoma (SDH), and hemorrhagic contusions in a 19-year-old man who was assaulted with a baseball bat following a road rage incident. His GCS score at presentation was 15. **(a)** Axial nonenhanced CT image shows multiple comminuted left-sided maxillofacial fractures (arrowhead) and a depressed fracture (arrow) of the squamosal segment of the left temporal bone. A left frontal bone fracture was also present (not shown). **(b–d)** Axial **(b, c)** and sagittal **(d)** nonenhanced CT images show a venous EDH anteriorly within the middle cranial fossa adjacent to the sphenoid bone fracture (arrow in **b** and **d**), a small arterial EDH associated with the depressed temporal bone fracture (straight arrow in **c**), and a shallow SDH (arrowheads in **c** and **d**) along the left frontal convexity. There were multifocal small hemorrhagic contusions (curved arrow in **c**) underlying the depressed temporal bone fracture.

a.

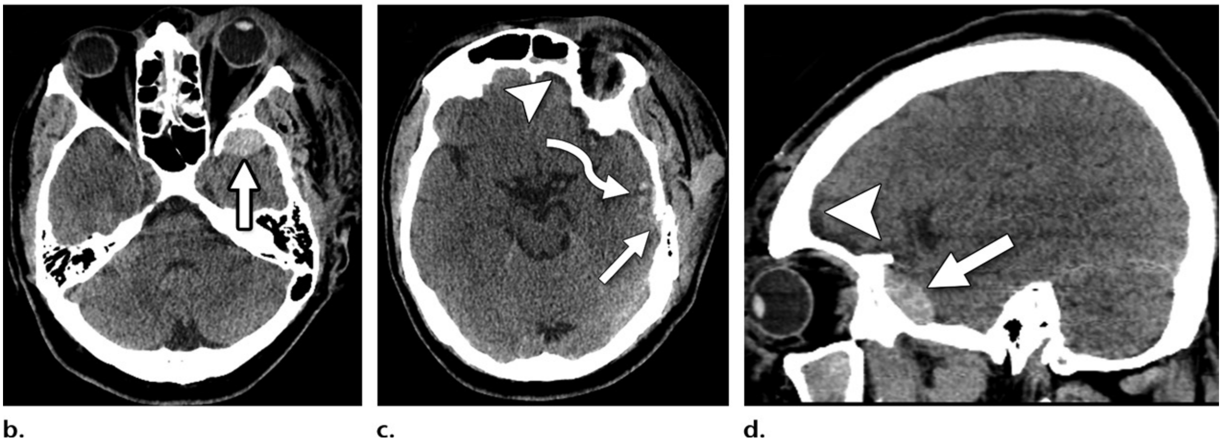

b. **c.** **d.**

the calvarium and skull base when necessary. The use of reformatted coronal and sagittal images maximizes diagnostic sensitivity for the detection of intracranial hemorrhage, extra-axial collections, and herniation (15).

MRI has substantially higher sensitivity than CT for the detection of EDH, SDH, nonhemorrhagic cortical contusions, brainstem injuries, and white matter axonal injuries (supported by level Ib evidence) (4,16–22). MRI is also more sensitive for the detection of hemorrhagic parenchymal contusions (level Ib–II evidence), all stages of SAH (level II evidence), and subacute SAH (level Ib–II evidence) (16–18,20–27).

A class I recommendation exists for MRI when nonenhanced CT is normal and there are persistent unexplained neurologic findings (4,28). However, in other clinical scenarios, the optimal role of MRI in TBI remains unclear, especially in light of safety concerns (eg, metallic foreign bodies), limited availability, longer imaging time, sensitivity to patient motion, and higher cost.

For adults, our nonenhanced brain MRI protocol includes performing diffusion-weighted and susceptibility-weighted imaging and fat-suppressed two-dimensional (2D) or 3D T2-weighted fluid-attenuated inversion-recovery (FLAIR), T2-weighted, and 2D or 3D T1-weighted sequences. The 3D sequences are acquired in the sagittal plane at 1-mm isotropic resolution and reformatted in the axial and coronal planes. Numerous studies have shown the higher sensitivity of susceptibility-weighted imaging over that of gradient-recalled-echo sequences for the detection of intracranial hemorrhage (29–33). Diffusion-weighted imaging is particularly important for the detection of nonhemorrhagic axonal injuries (34–37).

Imaging performed after the administration of contrast material (postcontrast) is not routinely performed in the trauma setting. However, early studies have shown that meningeal enhancement, a finding suggestive of meningeal injury, can be more sensitively detected with postcontrast T2-weighted FLAIR sequences (37–39).

Performing CT or MR angiography is recommended when a fracture traverses the carotid canal, in cases of penetrating injury, when there is concern for posttraumatic vasospasm, and when the intracranial hemorrhage pattern is atypical for trauma (11,40,41). Hemorrhage patterns that are atypical for trauma include isolated SAH in the basilar cisterns, isolated large-volume SAH in the sylvian fissure, and isolated SAH in the anterior interhemispheric fissure. Angiography should be considered in these cases to evaluate for a ruptured aneurysm (42). Additionally, a large hematoma with associated calcifications or prominent veins should raise suspicion for vascular malformation and

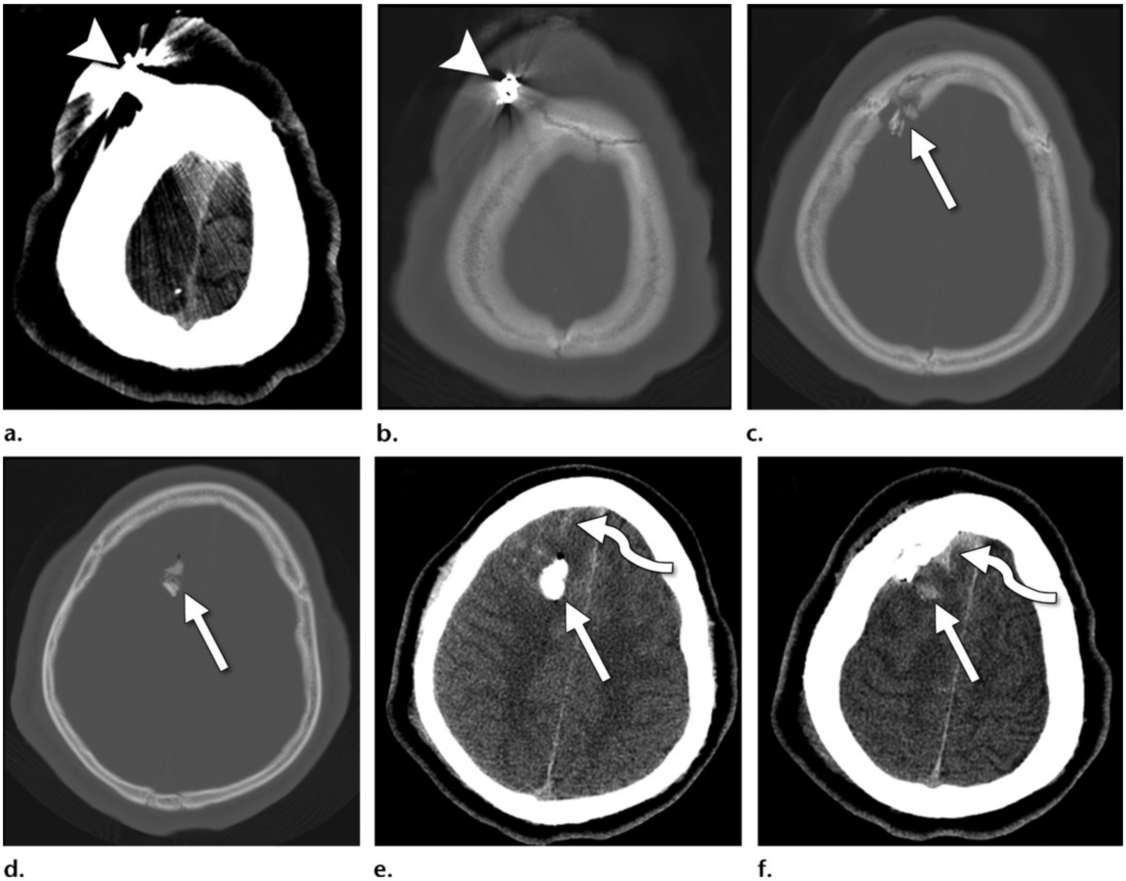

Figure 2. Penetrating trauma in a man shot with a .22-caliber bullet. **(a, b)** Axial nonenhanced brain window **(a)** and bone window **(b)** CT images show a bullet (arrowhead) that did not penetrate the skull. **(c–e)** Axial nonenhanced bone window **(c, d)** and brain window **(e)** CT images show a focal comminuted depressed right frontal bone fracture (arrow in **c**), with multiple bone fragments projecting into the right frontal lobe (straight arrow in **d, e**). **(f)** Axial nonenhanced CT image (brain window) shows a small associated right frontal lobe hemorrhagic contusion (straight arrow) and subarachnoid hemorrhage (SAH) (curved arrow in **e, f**).

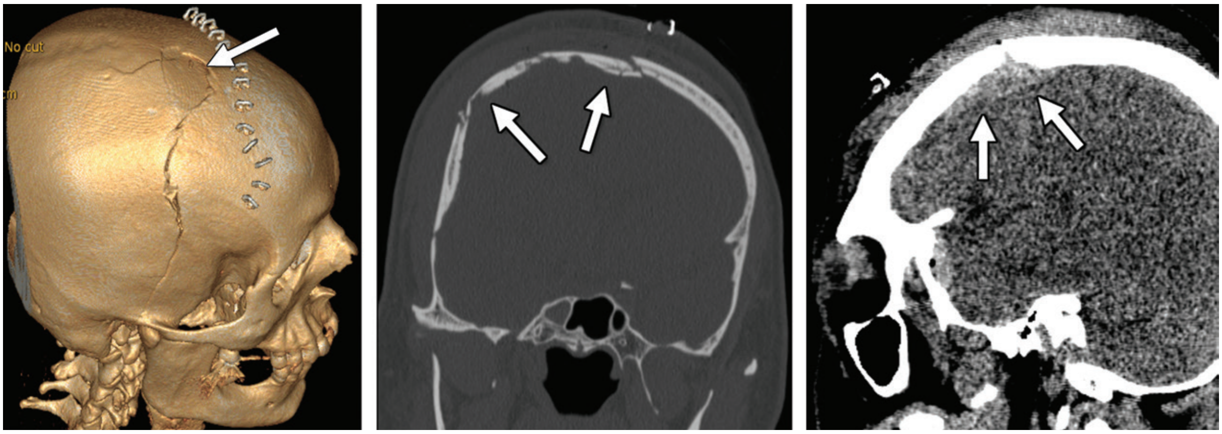

Figure 3. Focal depressed skull fracture in a young man who was hit on the head by a falling brick. Three-dimensional (3D) reconstructed (left) and coronal (middle) nonenhanced CT images show a focally depressed comminuted skull fracture (arrows). Sagittal CT image (right) shows an associated underlying small lentiform EDH (arrows). There was no hemorrhagic contusion or SAH.

should prompt angiography (42). CT or MR venography is helpful in cases where a fracture traverses a dural venous sinus, as these fractures are associated with venous EDHs and dural venous sinus thrombosis (43–47).

The ACR Appropriateness Criteria are evidence-based guidelines that describe the level of appropriateness in performing imaging studies for various clinical scenarios. Within the head trauma subsection of the neurologic

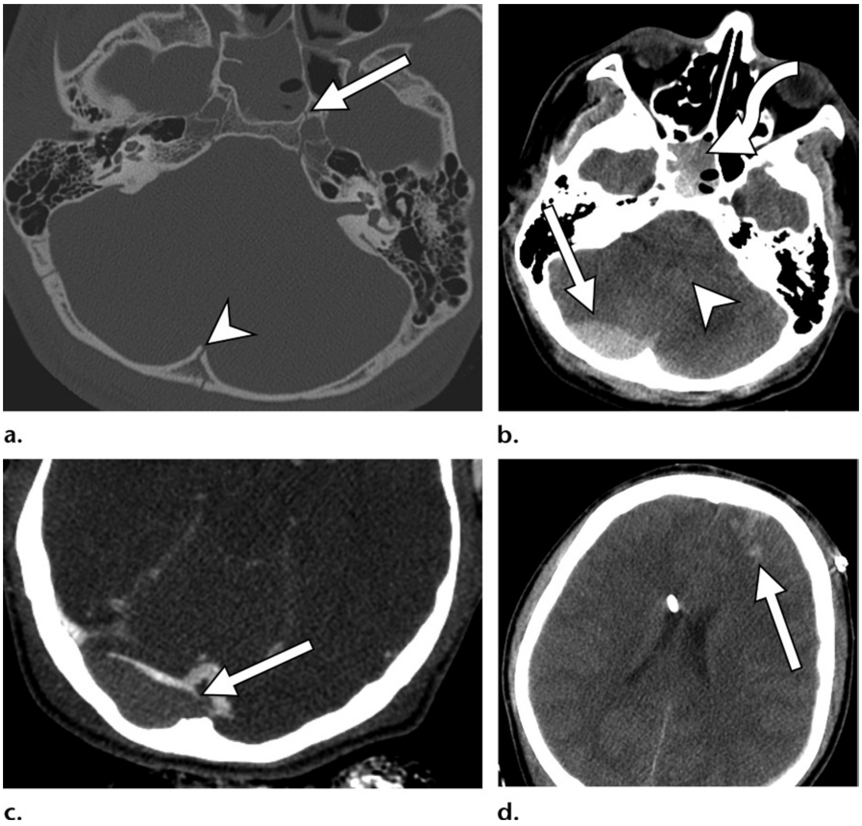

Figure 4. Posterior fossa occipital and skull base fracture with venous EDH in a 34-year-old man who was struck in the back of the head with a tire iron. His GCS score was 7. **(a)** Axial nonenhanced CT image shows a nondisplaced midline occipital bone fracture (arrowhead) extending through the left occipital condyle into the left petrous carotid canal and sphenoid sinus (arrow). **(b)** Axial nonenhanced CT image shows a lentiform venous EDH (straight arrow) causing regional mass effect, with compression of the fourth ventricle (arrowhead). Note the hemorrhage (curved arrow) within the sphenoid sinus related to the sphenoid fracture. **(c)** Axial nonenhanced CT venogram shows elevation and compression of the right transverse sinus and a probable venous laceration (arrow). **(d)** Axial nonenhanced CT image shows a focal contrecoup hemorrhagic contusion (arrow) in the left frontal lobe. A right frontal approach ventricular shunt catheter was emergently placed to treat the noncommunicating hydrocephalus and to decrease intracranial pressure.

criteria section, there are currently nine variant clinical scenarios (*https://acsearch.acr.org/list/GetAppendix?TopicId=139&PanelName=Neurologic*) with listings of the appropriateness of each applicable imaging modality (11). The criteria are frequently updated by expert panels on the basis of the peer-reviewed literature.

Diffusion-Tensor Imaging and Other Advanced Imaging Techniques

Growing awareness of the incidence and morbidity of TBI has led to extensive research in recent years to develop better diagnostic and prognostic imaging techniques. At the forefront, diffusion-tensor imaging (DTI) has been shown to be sensitive to the microstructural axonal injuries associated with mild TBI (48).

While DTI is currently valuable for group-based comparisons in the research arena, there are many barriers preventing the application of DTI in patients. While DTI is very sensitive to microstructural changes, there is a complete lack of specificity to relate findings to a specific cause. In the absence of premorbid imaging, diffusion-tensor images must be compared with images from normal controls for quantitative assessment. Increases in mean diffusivity and/or decreases in fractional anisotropy typically are interpreted to reflect decreased microstructural integrity of white matter in TBI studies. However, these same types of changes can be visualized in any number of comorbidities (49–51) or even demographic variation (52–56). As a result, accurate and meaningful interpretation of individual DTI examinations is not feasible.

Although outside the scope of this article, there are numerous additional barriers to the application of DTI in patients, which include *(a)* a lack of understanding of the normal range of variability in the population for DTI metrics; *(b)* the absence of an accepted robust analysis methodology suitable for individual use; *(c)* marked variability in DTI measurement owing to sequence parameter and hardware selection; *(d)* a paucity of multicenter trials establishing criteria for normal and abnormal findings; and *(e)* a lack of standardized methods for image acquisition, assessment, and interpretation. Each of these factors (ie, MR scanner type, sequence type, and analysis technique) cause variability in the mean diffusivity and fractional anisotropy measurements.

Newer forms of quantitative diffusion imaging are being continuously developed, which have been shown to provide a more detailed understanding of the diffusion properties in the brain. Some newer and more advanced techniques include diffusion-kurtosis (also called multishell DTI) (57), diffusion-spectrum (58), and restriction-spectrum (59) imaging and the application of biophysical models such as neurite orientation distribution and density

Figure 5. Skull base fracture, large anterior frontal hemorrhagic contusions, diffuse brain edema, herniation, and Duret hemorrhages in a 40-year-old woman who was hit by a car. Her GCS score was 3. **(a)** Axial nonenhanced head CT image shows a nondisplaced left occipital bone and skull base fracture (arrows) extending through the left carotid canal into the sphenoid sinus. No carotid injury was depicted at CT angiography (not shown). **(b)** Initial axial nonenhanced head CT image shows multifocal large hemorrhagic frontal lobe contusions (arrowheads) that increased at follow-up imaging. Temporal lobe contusions were also noted (not shown). Central downward herniation results in effacement of the suprasellar cistern and brainstem compression (arrow). **(c)** Axial nonenhanced head CT image shows global brain edema with diffuse loss of the cerebral sulci. **(d)** Axial nonenhanced CT image shows a left frontal approach ventriculostomy catheter, which was placed emergently. Decompressive bilateral craniectomies were immediately performed. Short-term interval follow-up MRI was performed because the patient remained in a persistent vegetative state. **(e–g)** Axial T2-weighted **(e, f)** and susceptibility-weighted **(g)** MR images show the expected involutional changes within the frontal and temporal lobes from the hemorrhagic contusions (arrows) and developing hydrocephalus from the SAH **(f)**. **(h)** Axial susceptibility-weighted MR image shows large Duret hemorrhages (arrow) within the mid- and dorsal pons, a sequela of herniation.

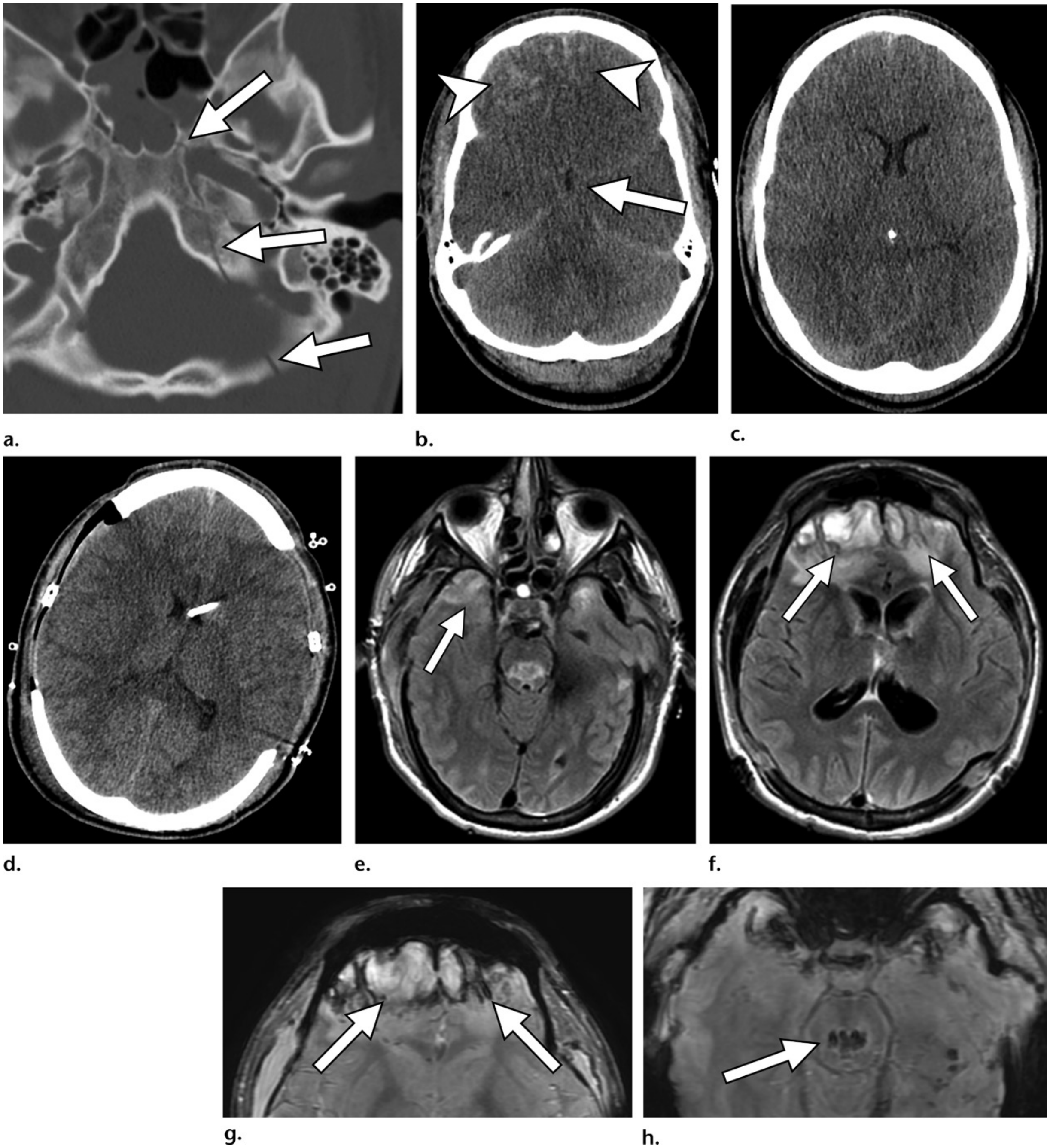

imaging (60). These techniques may yield better sensitivity and specificity in the future.

National efforts are underway to tackle existing barriers to clinical use, such as variation owing to hardware and understanding of normal population variability. There is great promise that a form of quantitative diffusion imaging will be a suitable biomarker for mild TBI in the future, but it currently remains investigational and not applicable for the assessment of patients.

Prognostic Utility

Obtaining initial head CT images has prognostic implications. The Rotterdam, Marshall, Stockholm, and Helsinki CT scores are among the tools that have been used to predict mortality at 6 months (61,62). More recently, the NeuroImaging Radiological Interpretation System has been used to grade the severity of acute TBI (63). Among patients with a GCS score of 15, 6.9% had acute findings at head CT in a seminal article (12). A recent meta-analysis of patients with complicated mild TBI (GCS scores of 13–15) found that acute traumatic findings on head CT images are important for both management and prognosis, as there are low but clinically important rates of clinical deterioration (11.7%), neurosurgical intervention (3.5%), and death (1.4%) in this subpopulation of patients with mild TBI (64). Quantitative CT may further improve prognostication over qualitative CT interpretation in cases of acute TBI (65). Quantitative CT refers to the use of computer-aided image analysis to quantify the volume of hemorrhage in different compartments, volume of the basilar cisterns, and degree of midline shift (65). Yuh et al (65) found that use of quantitative CT on admission head CT studies resulted in improved ability to predict the 6-month Extended Glasgow Outcome Scale (GOS-E) score in patients with TBI (65).

The prognostic value of MRI in addition to that of CT is an area of active investigation, but early findings from the prospective Traumatic Research and Clinical Knowledge in TBI (TRACK-TBI) study suggest added prognostic value (66). Specifically, cases of one or more contusions at MRI or at least four foci of hemorrhagic axonal injury were associated with worse clinical outcome at 3 months on the GOS-E even when controlling for CT findings and demographic, socioeconomic, and clinical factors (66). A separate study evaluating patients with severe TBI found that the addition of MRI features improved prognostication for outcome after 1 year in patients with severe TBI (67). A recent systematic review and meta-analysis of early MRI in cases of moderate and severe TBI suggested added prognostic value with lesions detected at MRI, but most studies included were at high risk of bias (68).

Standardized Reporting and Data Collection for TBI

The TBI Reporting and Data System (TBI-RADS) (69), an initiative of the ACR Head Injury Institute (70), is part of a greater national effort led by the ACR to standardize reporting and data collection for TBI and create an evidence-based management scheme for patient disposition. This system will undergo continuous revision as newer data and additional evidence are collected and analyzed. At present, TBI-RADS incorporates three features: *(a)* acute head CT findings, *(b)* demographic information, and *(c)* focused medical history and/or physical examination findings.

The most immediate potential implication for this system is to stratify the disposition of patients with acute TBI. The goal is to use current evidence to determine which patients can be safely discharged with close follow-up, those who should be admitted to a non–intensive care unit (ICU) floor as a precaution, those who need close monitoring in the ICU, and those who require immediate surgery. Standardizing reporting and management have multiple benefits, including allowing data to be pooled easily from multiple institutions and care centers. By stratifying the disposition of patients with acute TBI, there is a potential for considerable nationwide health care savings in terms of both money and resources.

Additional benefits include creating a template for education across disciplines and a standardized system to create use cases for the development of artificial intelligence and deep learning algorithms. It is the goal of TBI-RADS to reduce interpretation variability and errors, enhance communication with ordering clinicians, facilitate quality improvement and research, and ultimately improve outcomes of patients with TBI (71).

Injury Types and Imaging Findings in TBI

Skull Fracture

Skull fractures can be caused by blunt (Fig 1) or penetrating (Fig 2) injury and frequently tear the underlying meninges if depressed (Fig 3). Anterior cranial fossa fractures are frequently associated with a CSF leak, especially when comminuted or oblique (72). Fractures that traverse a dural venous sinus (Fig 4) or the jugular bulb are associated with injury to the underlying vein in two-thirds of cases (43). This is commonly due to extrinsic compression caused by extra-axial hematoma (in particular a venous EDH as seen in Fig 4) and/or thrombosis (which occurs in 23%–41% of cases) (43–47). Fractures extending to a suture can be associated with diastasis, especially in children. Skull base fractures (Fig 5) are beyond the scope of this article, but imaging of temporal bone trauma in the emergency setting has been previously reviewed (73).

Epidural Hematoma

EDHs occur between the inner table of the skull and the superficial layer of the dura and are often

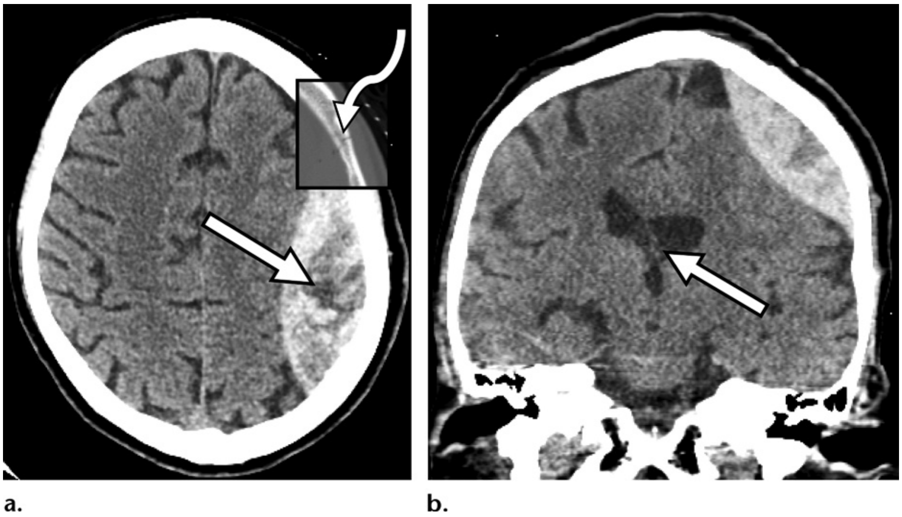

Figure 6. Hyperacute EDH with swirl sign in a middle-aged woman who fell and struck her head while walking down stairs. Her GCS score was 15. **(a)** Axial nonenhanced head CT image shows a large lentiform left frontoparietal convexity EDH that does not cross the coronal or lambdoid sutures. A subtle fracture is best visualized on the bone window image inset (curved arrow in inset). Mixed low-attenuation internal blood products are findings compatible with hyperacute nonclotted hemorrhage, otherwise known as the swirl sign (straight arrow). **(b)** Coronal nonenhanced head CT image shows regional mass effect on the left parietal lobe with compression of the left lateral ventricle and mild rightward subfalcine shift (arrow), which are best appreciated on the coronal reformatted image.

lenticular in shape (Fig 6). EDHs typically do not cross suture lines as the superficial dural layer is attached to the calvarium tightly along the sutures (74). In the rare case in which the fracture involves the suture (more common in children), one may visualize the EDH crossing the suture line (Fig 7).

EDHs can accumulate owing to arterial or venous hemorrhage. In the pterional region, arterial EDHs classically arise from the middle meningeal artery. If there is an internal hypoattenuating component (swirl sign), this suggests active bleeding (Fig 6) (75). Venous EDHs can occur when the fracture crosses a dural venous sinus (Fig 4) and can cross the falx cerebri and tentorium cerebelli. The source of a vertex venous EDH is typically the superior sagittal sinus. The source of an anterior temporal EDH is the sphenoparietal sinus (Fig 8). These have a more benign course and do not require surgery as they are limited by the sphenotemporal suture and the orbital fissure (76). EDHs can be treated with surgical evacuation or middle meningeal artery embolization for stabilization of nonsurgical small- to medium-sized EDHs (77).

Subdural Hematoma

SDHs occur between the dura and arachnoid mater, are most commonly caused by a tear in a bridging cortical vein as it crosses the dura, and can cross suture lines but not the falx or tentorium, as these are dural reflections (74). The general progression of SDHs from acute to chronic is the appearance progressing from hyper- to hypoattenuating. However, there are a number of potential pitfalls to assigning an SDH an age based only on attenuation. It is important to note that mixed-attenuation SDHs are not necessarily acute on chronic. The hypoattenuating portions may represent hyperacute and/or unclotted chronic blood products, particularly in patients with coagulopathy. Furthermore, SDHs that are isoattenuating relative to the brain parenchyma can be acute, for example, in a profoundly anemic patient or in a patient with an arachnoid tear and a mixture of hemorrhage and CSF.

A large meta-analysis showed substantial overlap in the CT and MRI appearances of SDHs of different ages, with hyperattenuating and mixed-attenuating SDHs reported after a median interval of 1–2 days, isoattenuating SDHs reported after a median interval of 11 days, and hypoattenuating SDHs reported after a median interval of 14 days (78).

In the subacute stage, membranes composed of granulation tissue can form within the hematoma (Fig 9). These types of membranes can enhance. In subacute-to-chronic SDHs, the membranes are friable and can result in recurrent hemorrhage, resulting in an acute-on-chronic SDH. This will often show hematocrit levels (Fig 9). Chronically, calcifications can form. SDHs can be treated with burr hole drainage, craniotomy for evacuation, subdural evacuation port system (Fig 10) placement, and/or middle meningeal artery embolization (79,80).

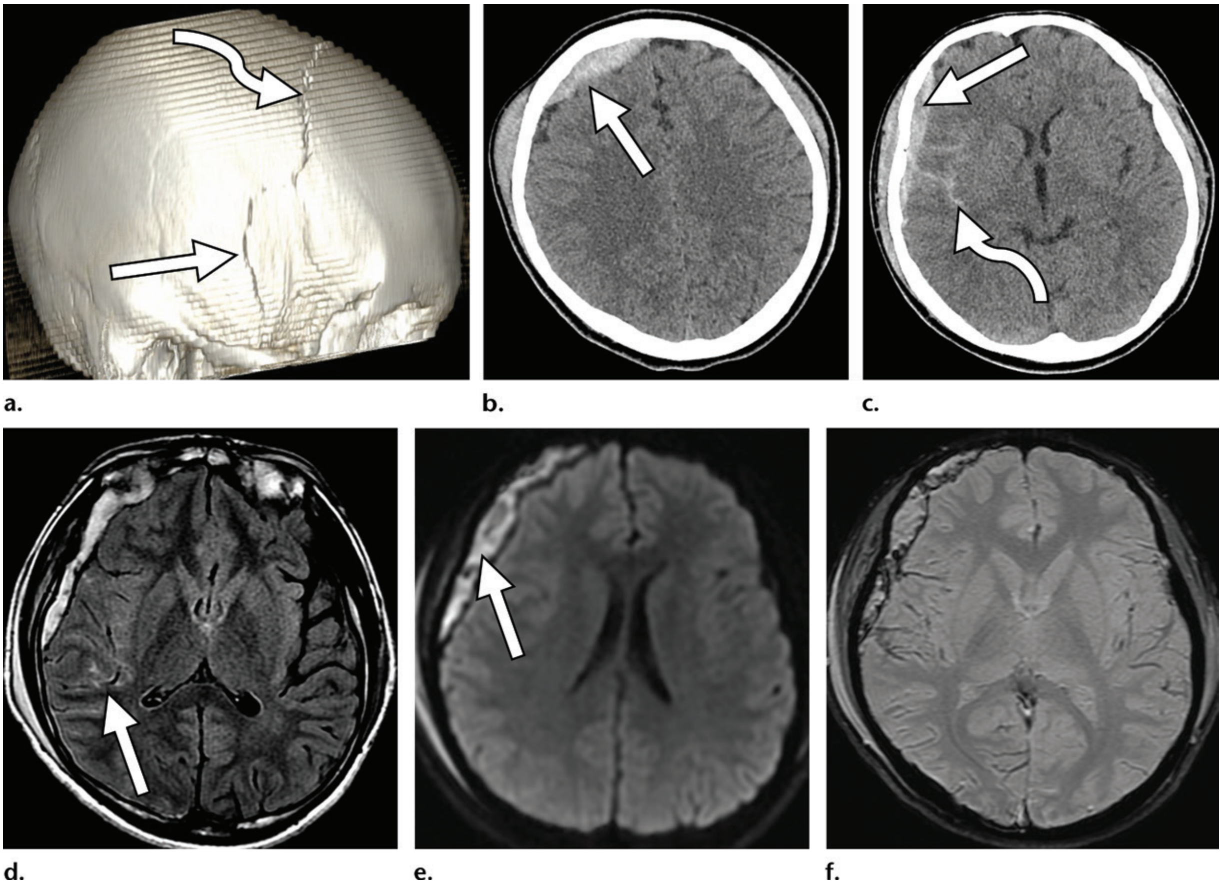

Figure 7. Mixed hyperacute and acute EDH associated with calvarial fracture and coronal suture diastasis in a 24-year-old man with a large right temporoparietal scalp hematoma following assault. His GCS score was 15. **(a)** 3D volume-rendered nonenhanced reconstructed head CT image shows a nondisplaced right parietotemporal fracture (straight arrow) extending into the coronal suture, which was diastatic (curved arrow). **(b, c)** Axial nonenhanced CT images show a bilobular lentiform hyperacute and acute EDH (straight arrow) along the right frontal and temporal convexities. Mixed low- and high-attenuating blood products within the temporal component of the EDH are suggestive of active bleeding and/or unclotted hemorrhage. Note the SAH (curved arrow in **c**) within the right sylvian fissure. **(d)** Axial T2-weighted FLAIR MR image obtained at follow-up shows residual SAH (arrow). **(e)** Axial diffusion-weighted image shows evolving subacute blood products (arrow), with restricted diffusion within the EDH. Mass effect is mildly decreased, with less compression of the right lateral ventricle. **(f)** Axial susceptibility-weighted image does not show any associated contusions or traumatic axonal injury (TAI).

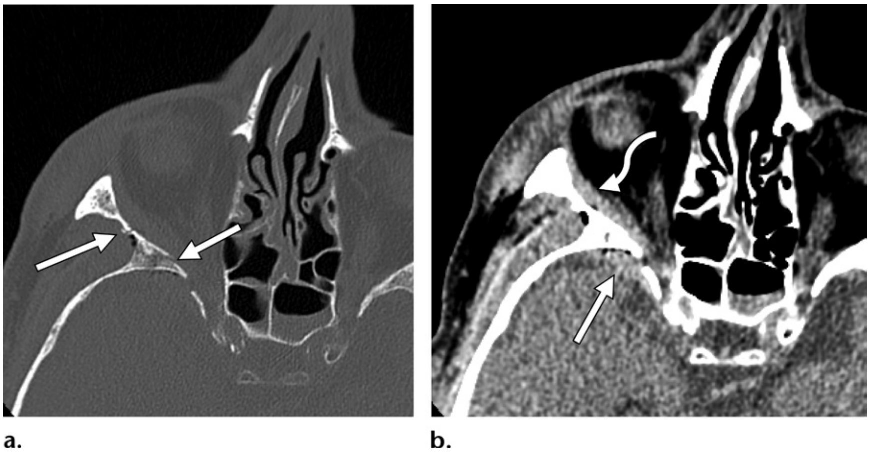

Figure 8. Zygomaticosphenoid fracture with sphenoparietal venous EDH and intraorbital subperiosteal hematoma in a 78-year-old woman who fell on the right side of her face. Her GCS score was 15. **(a)** Axial maxillofacial CT image (bone window) shows comminuted right zygomatic and sphenoid bone fractures (arrows) with air in the temporalis fossa, a right cheek hematoma, and right exophthalmos. **(b)** Axial maxillofacial CT image (soft-tissue window) shows a small venous EDH (straight arrow) along the anterior middle cranial fossa related to traumatic laceration of the sphenoparietal sinus. Note the extraconal intraorbital subperiosteal hematoma (curved arrow).

Figure 9. Posttraumatic mixed-signal-intensity SDH resulting in cerebral herniation in an elderly man undergoing anticoagulation therapy who fell at home 2 weeks earlier and presented with progressive right-sided headache. **(a–c)** Axial MR images show a large complex mixed-signal-intensity crescentic right hemispheric SDH. Predominately T1-hyperintense (arrow in **a**) and T2-hyperintense (arrow in **b**) late subacute internal blood products are depicted, with hemosiderin-stained internal septa on the susceptibility-weighted image (arrow in **c**), a finding suggestive of recurrent internal hemorrhage. There is a layering hematocrit level (arrowheads in **a**, **b**) posteriorly, compatible with poor coagulation. **(d)** Coronal postcontrast T1-weighted MR image shows significant mass effect on the right cerebrum with mild leftward subfalcine herniation (straight arrow) and early right uncal herniation (curved arrow). Note the secondary dural inflammation and intrasulcal linear enhancement (arrowheads), representing venous congestion. Postcontrast imaging is not routinely performed in the trauma setting, but these findings should not be mistaken for other pathologic conditions such as infection.

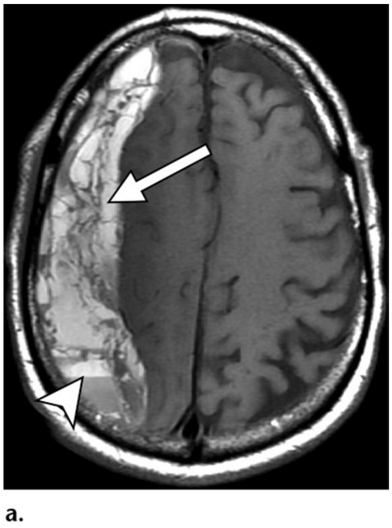

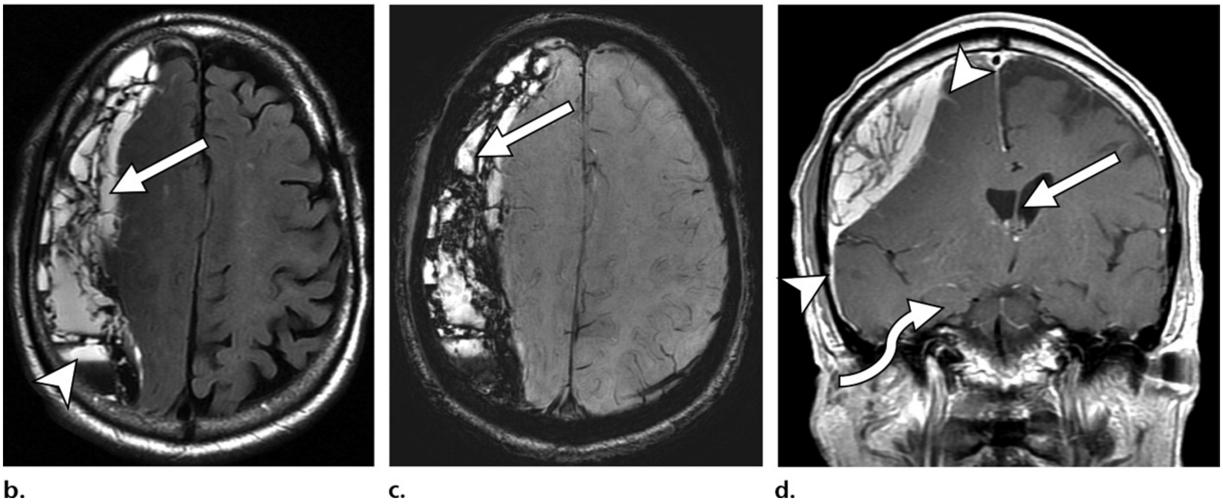

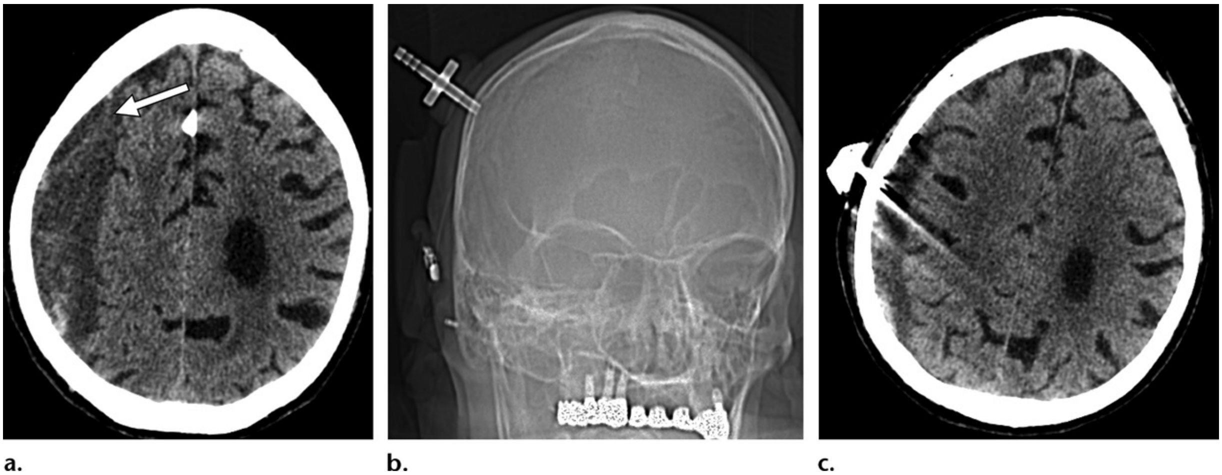

Figure 10. Subdural evacuating port system (SEPS) in an 82-year-old woman with a GCS score of 14 following a fall in the bathtub. **(a)** Axial nonenhanced head CT image shows a large acute-on-chronic SDH (arrow) containing mixed internal hemorrhage of varying densities and internal septa. Note the moderate mass effect on the right cerebral hemisphere. **(b)** CT scout image obtained following SEPS placement shows the device. **(c)** Axial nonenhanced head CT image shows a resultant decrease in the size of the SDH and cerebral compression.

Figure 11. Enlarging frontal lobe contusion and subdural hygromas in an elderly woman who fell down stairs and was diagnosed with a right frontal scalp contusion. Her GCS score was 13. **(a, b)** Initial axial nonenhanced head CT image **(a)** shows a small nonhemorrhagic anterior right frontal contusion (arrow) that increased in size and conspicuity on the follow-up nonenhanced head CT image **(b)** obtained 12 hours later. **(c, d)** Coronal nonenhanced head CT image **(c)** shows trace right and small left hemispheric subdural hygromas (arrows), which increased on the follow-up coronal nonenhanced head CT image **(d)**. **(e, f)** Axial T2-weighted FLAIR **(e)** and susceptibility-weighted **(f)** MR images obtained the next day show the anterior right frontal contusion (arrow in **e**) with internal microhemorrhage (arrow in **f**). The internal microhemorrhages were not appreciable on the nonenhanced CT images. **(g)** Axial T2-weighted FLAIR MR **(g)** and diffusion-weighted **(h)** images show bilateral enlarging small subdural hygromas (arrows in **g**) and focal restricted diffusion (arrow in **h**) within the left occipital white matter. The focus of restricted diffusion in the left occipital white matter suggests a contrecoup TAI.

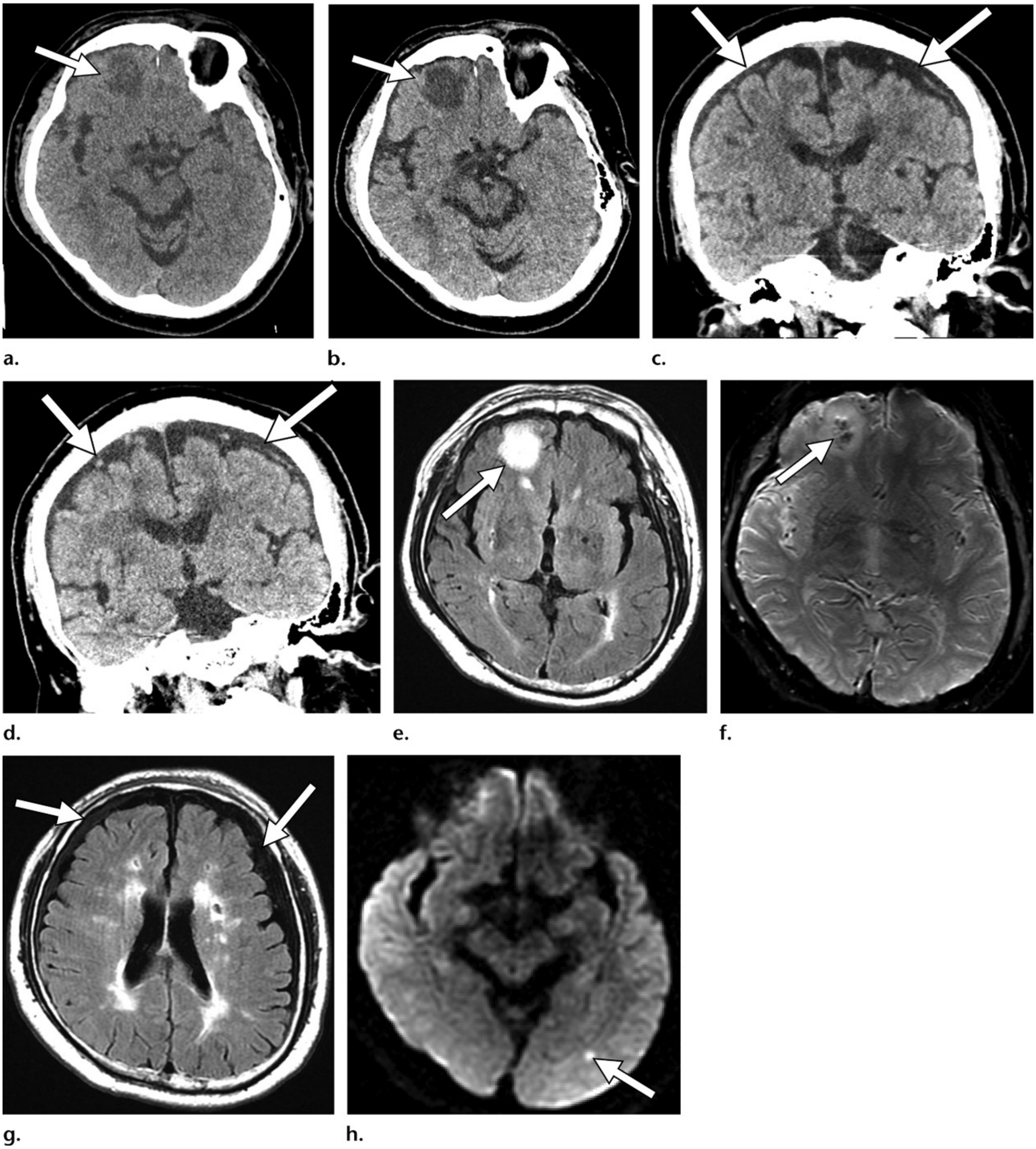

Subdural Hygroma

Subdural hygromas are caused by traumatic tears in the arachnoid membrane with resulting CSF accumulation in the subdural space and can coexist with other findings of intracranial injury (Fig 11) (81). As depicted in all subdural collections, hygromas displace vessels in the subarachnoid space from the inner table of the calvarium, but this finding is particularly important for the diagnosis of a subdural hygroma, as the fluid will be isoattenuating and isointense relative to CSF on CT and MR images, respectively. One

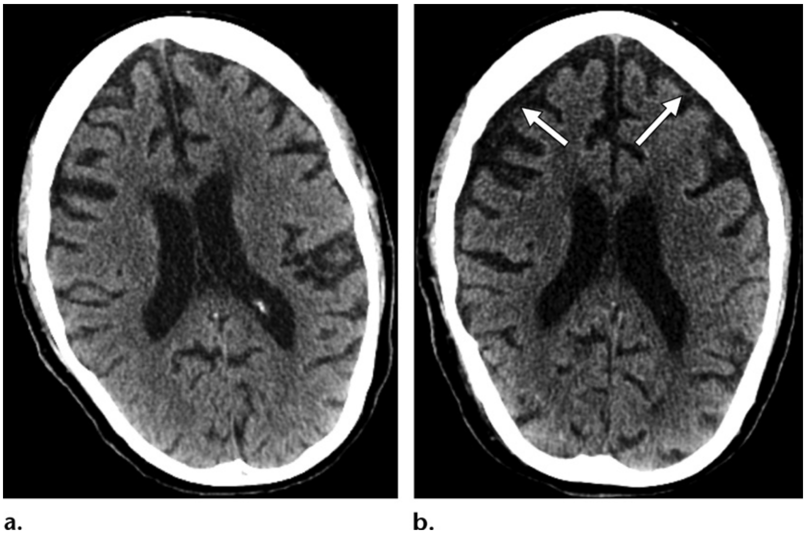

Figure 12. Delayed subdural hygromas. **(a)** Axial nonenhanced head CT image in an elderly patient following a mild TBI was interpreted as normal. The patient presented 6 days after discharge with persistent headache. **(b)** Axial nonenhanced head CT image obtained at follow-up shows new small posttraumatic subdural hygromas (arrows), causing minimal mass effect on the cerebral hemispheres. There is no herniation owing to the preexisting global brain atrophy.

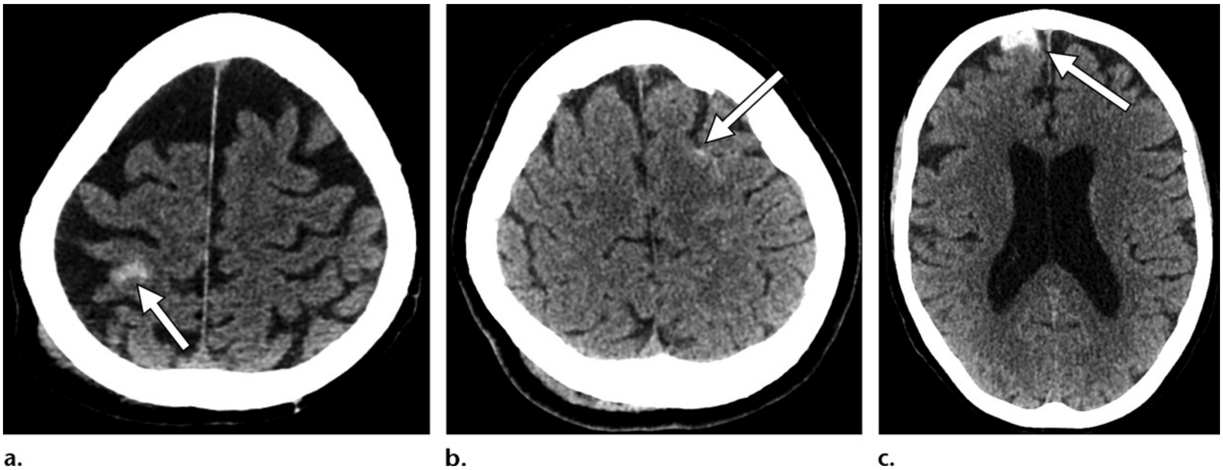

Figure 13. Posttraumatic SAH in three patients with minor head injuries whose GCS score was 15. Axial nonenhanced CT images show small amounts of SAH in coup (arrow in **a**) and contrecoup (arrow in **b**, **c**) patterns.

exception has been demonstrated in polytrauma patients who received intravenous contrast material during initial evaluation. Subsequent head CT images depicted subdural collections that were hyperattenuating relative to CSF on 120-kVp images but isoattenuating relative to CSF on virtual monoenergetic 190-keV images. This confirmed that not hemorrhage but iodine was the source of hyperattenuation on 120-kVp images (82).

Subdural hygromas can occur in the first day, but the mean time to appearance is 9 days after injury (Fig 12) (81). A pure subdural hygroma will not have internal membranes as can subacute SDHs (81). However, subdural CSF accumulation can occur with hemorrhage, particularly in children, resulting in a hematohygroma (83,84). Of note, subdural effusions are secondary to reactive fluid accumulation in the subdural space (eg, owing to meningitis) and should not be confused with subdural hygromas.

Traumatic SAH

Traumatic SAH occurs between the arachnoid and pia mater and is a usually small-volume sulcal SAH (Fig 13) that commonly occurs at the site of impact (coup) or opposite the site of impact (contrecoup). Patients with isolated traumatic SAH are less likely to clinically deteriorate than those with other types of traumatic intracranial hemorrhage (85). However, evidence shows impaired functional outcomes in patients with traumatic SAH. In the European Brain Injury Consortium survey (86), 41% of patients without traumatic SAH achieved good recovery, whereas 15% of patients with traumatic SAH achieved good recovery. Midline traumatic SAH (in the interhemispheric fissure or perimesencephalic cisterns) on initial head CT images (Fig 14) is a marker of diffuse axonal injury (DAI) at subsequent MRI, with a 61% sensitivity and 82% specificity for severe DAI in one study (87).

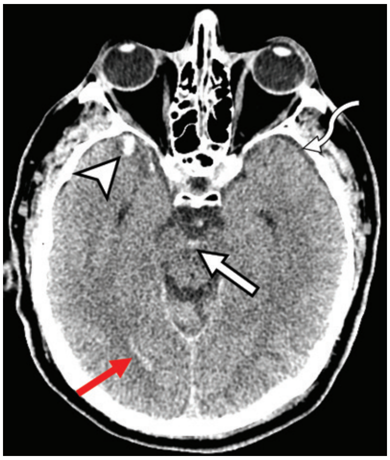

Figure 14. Interpeduncular hemorrhage, intraventricular hemorrhage, and temporal lobe hemorrhagic contusion in a 24-year-old woman who was struck by a car and presented with loss of consciousness. Her GCS score was 8. Initial axial nonenhanced head CT image shows multicompartmental hemorrhages. Interpeduncular SAH (white arrow), intraventricular hemorrhage (red arrow), and a small focal hemorrhagic contusion (arrowhead) in the anterior right temporal lobe are depicted. Note the small left temporal convexity subdural hygroma (curved arrow).

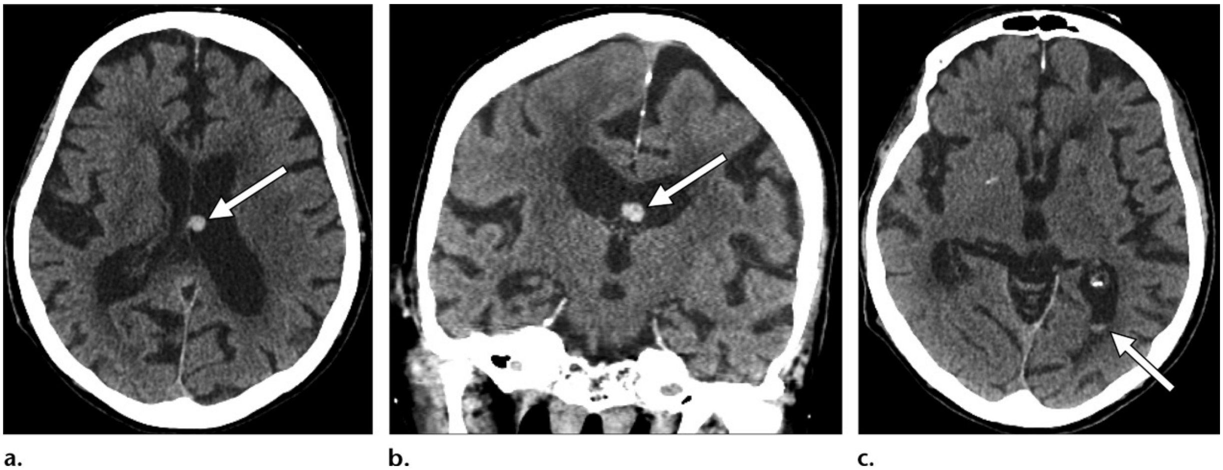

Figure 15. Traumatic septum pellucidum hemorrhage in an elderly woman following a fall from standing. Her GCS score was 13. **(a, b)** Axial **(a)** and coronal **(b)** nonenhanced head CT images show a focal hemorrhage (arrow) along the septum pellucidum, most likely related to a lacerated septal vein. **(c)** Axial nonenhanced CT image shows a small amount of associated intraventricular hemorrhage (arrow).

Isolated SAH in the basilar cisterns should prompt consideration of aneurysmal SAH, even in the setting of trauma. Traumatic SAH in the interpeduncular or perimesencephalic cisterns should raise suspicion for brainstem injury (88). Rarely, traumatic SAH can cause delayed vasospasm, although much less frequently than aneurysmal SAH. The risk of posttraumatic vasospasm is highest in severe TBI, where it occurs in up to 30%–40% of patients (41).

Intraventricular Hemorrhage

Intraventricular hemorrhage in the setting of trauma (Fig 14) can originate from a ruptured subependymal vein (Fig 15), extension from an intraparenchymal hematoma, or retrograde redistribution from the subarachnoid space. Intraventricular hemorrhage on initial head CT images is correlated with DAI on subsequent MR images, with univariate and multivariate odds ratios of 3.7 and 4.2, respectively, shown in one study (89).

Brain Contusion

Brain contusions are bruises of the brain parenchyma owing to impact. They characteristically occur at coup and contrecoup sites, most commonly in the inferior frontal lobes and anterior-inferior temporal lobes, thought to be due to the ridged morphology of the inner table, with a predilection for the crests of the involved gyri (Fig 16). Temporal lobe contusions on CT images are associated with worse functional outcome at 6 months than that of frontal lobe contusions, other intra-axial injuries, or extra-axial injuries (90). MRI is more sensitive than CT for the detection of contusions, especially small or nonhemorrhagic contusions (20,91). Contusions can increase in size (ie, "blossom" or "bloom") over the first 48 hours after injury (Fig 17) (92). Significant progression of contusions (new contusion or doubling in contusion volume) is associated with worse clinical outcome (93).

Contusions are followed with serial imaging, and in cases where hemorrhagic progression leads to increasing mass effect and herniation, craniectomy

Figure 16. Classic evolving bifrontal hemorrhagic contusions, frontal SDHs, diffuse brain swelling, SAH, and intraventricular hemorrhage in a 58-year-old patient who was struck by a car while cycling. The patient's GCS score was 13. **(a–d)** Axial **(a–c)** and coronal **(d)** nonenhanced CT images show bifrontal hemorrhagic contusions (arrows in **a**, **d**), small bifrontal SDHs (arrowheads in **b**), right occipital intraventricular hemorrhage (curved arrow in **b**), and multifocal SAH (arrows in **c**). **(e–g)** Axial nonenhanced CT images obtained a few days later show the expected interval evolution of the bifrontal hemorrhagic contusions, with decreased internal hemorrhage but persistent edema (arrows in **e**). Note the decrease in internal hemorrhage but an increase in the size of the bifrontal SDHs (arrowheads in **f**). Intraventricular hemorrhage increased (curved arrow in **f**) and SAH resolved **(g)** owing to redistribution. The lateral ventricles increased in size over time, which was thought to be related to interval decrease in diffuse brain swelling. **(h)** Coronal nonenhanced CT image also shows increased edema and decreased hemorrhage within the bifrontal hemorrhagic contusions (arrows) and a slight increase in the size of the bifrontal SDHs (arrowheads).

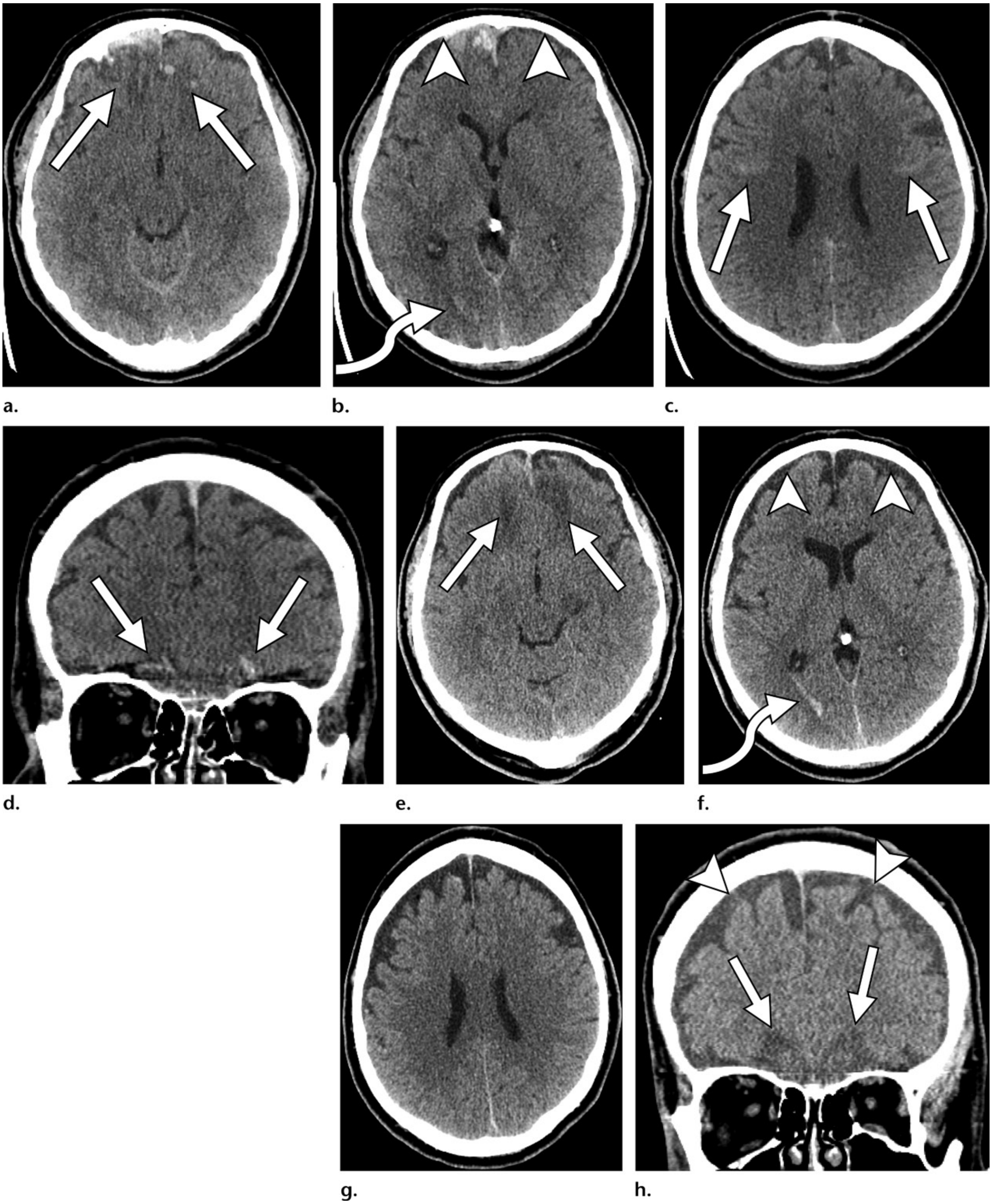

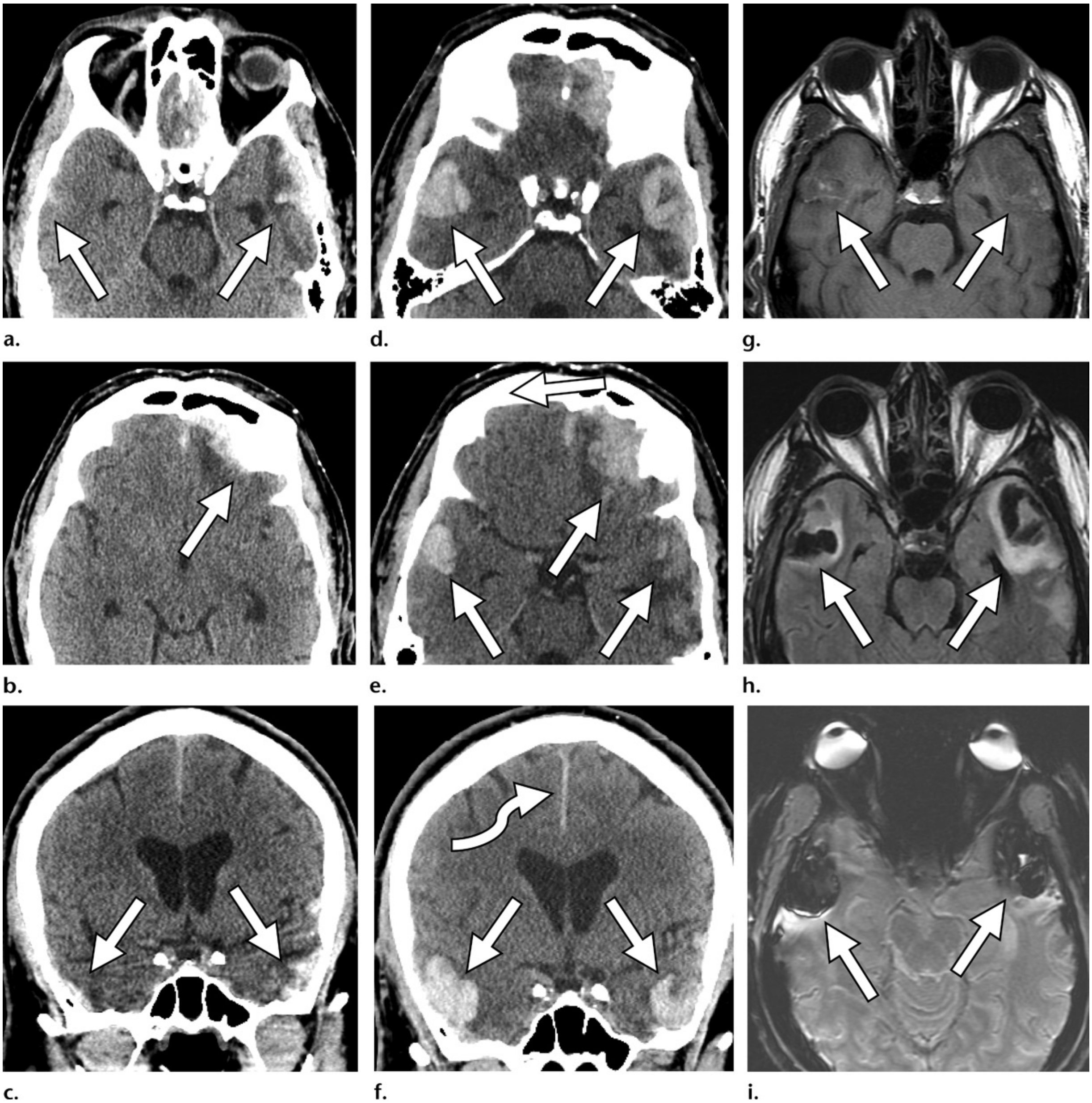

Figure 17. Enlarging hemorrhagic bilateral frontal and temporal lobe contusions in a 62-year-old woman who was thrown from a horse. Her GCS score was 6. **(a–c)** Initial axial **(a, b)** and coronal (**c**) nonenhanced head CT images show multifocal relatively small superficial hemorrhagic contusions (arrows) of the anterior temporal lobes and anteroinferior left frontal lobe, a pattern highly typical for moderate to severe TBI. **(d–f)** Axial **(d, e)** and coronal (**f**) nonenhanced head CT images obtained 24 hours later show a marked interval increase in the size of the hemorrhagic contusions (straight arrows) and the resultant mass effect without herniation. Note a small anterior parafalcine SDH (curved arrow in **f**) that has slightly increased in size. **(g–i)** Axial MR images obtained at short-term interval follow-up do not show evidence of TAI, but evolving acute to early subacute blood products (arrows) are depicted on the T1-weighted MR image (**g**) (with iso- to hyperintense signal), T2-weighted FLAIR image (**h**) (with predominately hypointense signal), and susceptibility-weighted image (**i**) (with hypointense signal).

may be performed to prevent the secondary effects of herniation described later in this article. Severe acceleration and/or deceleration or rotational injury can result in brainstem contusions (eg, when the midbrain or superior cerebellar peduncle impacts the tentorial incisura) (Fig 18) (94).

Axonal Injury

Axonal injuries result from axonal stretch and/or shear stress and predominantly affect highly organized white matter tracts and interfaces between brain tissues of different densities (ie, gray-white junction). There has been variable use of two related terms, *TAI* and *DAI*, and they are often used interchangeably. DAI is historically used to describe widespread multifocal white matter injury as a result of shearing forces from rotational and translational acceleration-deceleration injuries confirmed by pathologic studies demonstrating axonal

Figure 18. Frontal bone fracture in a 48-year-old man who tripped, fell, and hit a concrete ledge. He was diagnosed with persistent right pupillary mydriasis. His GCS score was 15. **(a)** Axial nonenhanced head CT image and bone-window image (inset) show a nondisplaced right frontal bone fracture (arrow in inset), which is best depicted on the bone-window image. No intracranial hemorrhage or contusion is depicted. **(b–d)** Sagittal T2-weighted FLAIR MR image **(b)** obtained at follow-up shows a focal hemorrhagic contusion (straight arrow in **b**) of the right superior cerebellar peduncle, with focal restricted diffusion (arrow in **c**) on the axial diffusion-weighted image **(c)** and microhemorrhage (arrow in **d**) on the axial susceptibility-weighted image **(d)**. Note the mild increased signal intensity in the right oculomotor nerve (curved arrow in **b**), a finding compatible with a traumatic cranial nerve injury, which explains the manifestation of mydriasis.

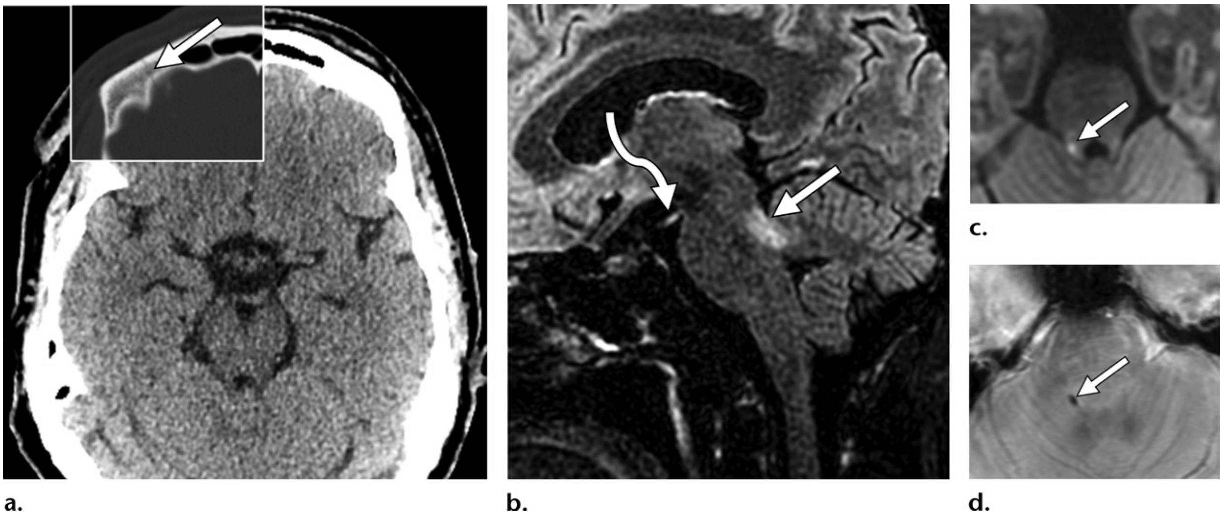

Figure 19. Focal mild acute axonal injury in a 34-year-old-woman who was an unrestrained passenger in the backseat during a motor vehicle collision. She presented with severe headache and confusion. Her GCS score was 14. **(a)** Axial nonenhanced head CT image shows no abnormal findings. Short-term MRI was performed owing to persistent confusion. **(b)** Axial susceptibility-weighted MR image shows two foci (arrows) within the anterior right frontal white matter. **(c)** Axial postprocessed quantitative susceptibility map shows positive phase shifts (arrows) corresponding to the presence of internal ferromagnetic iron. **(d)** Axial diffusion-weighted image shows no associated abnormality. **(e)** Axial T2-weighted FLAIR image shows focal T2-hyperintense lesions (arrows), findings compatible with gliosis, that correspond to microhemorrhages.

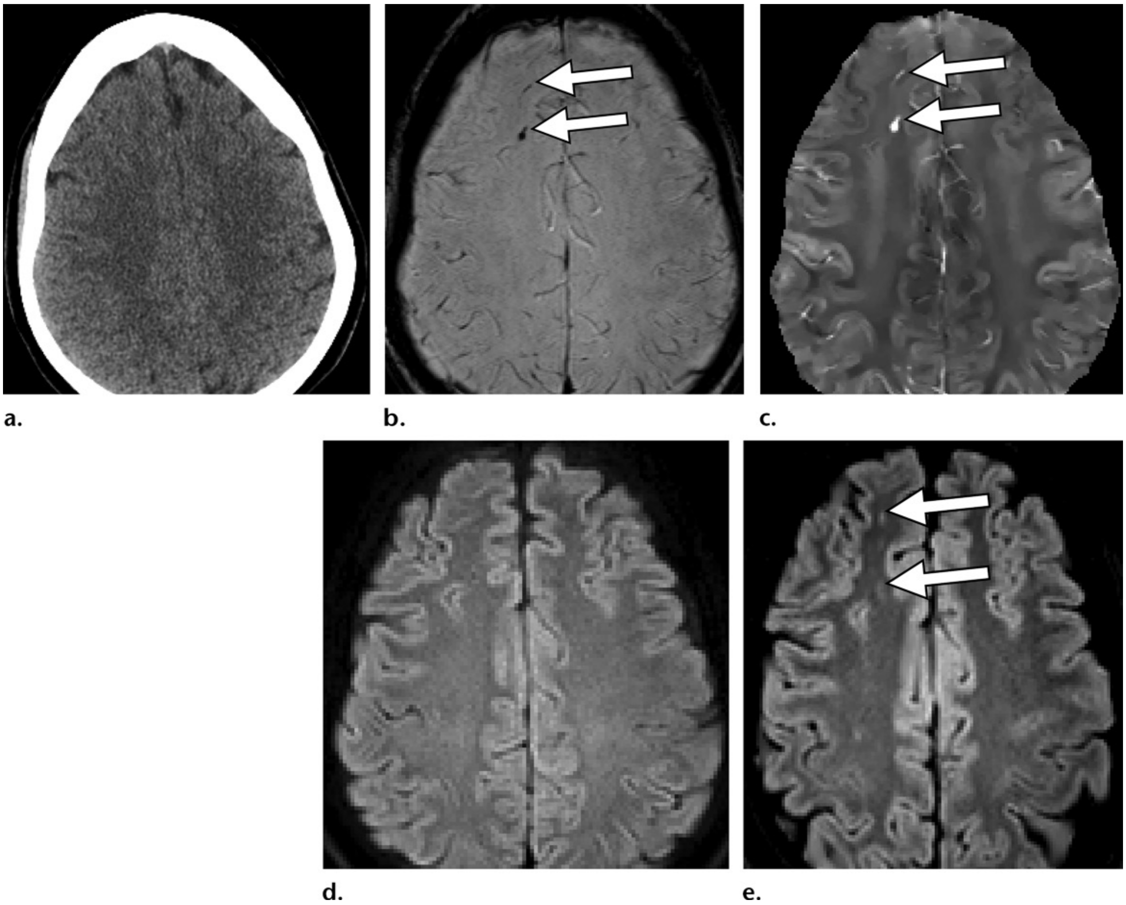

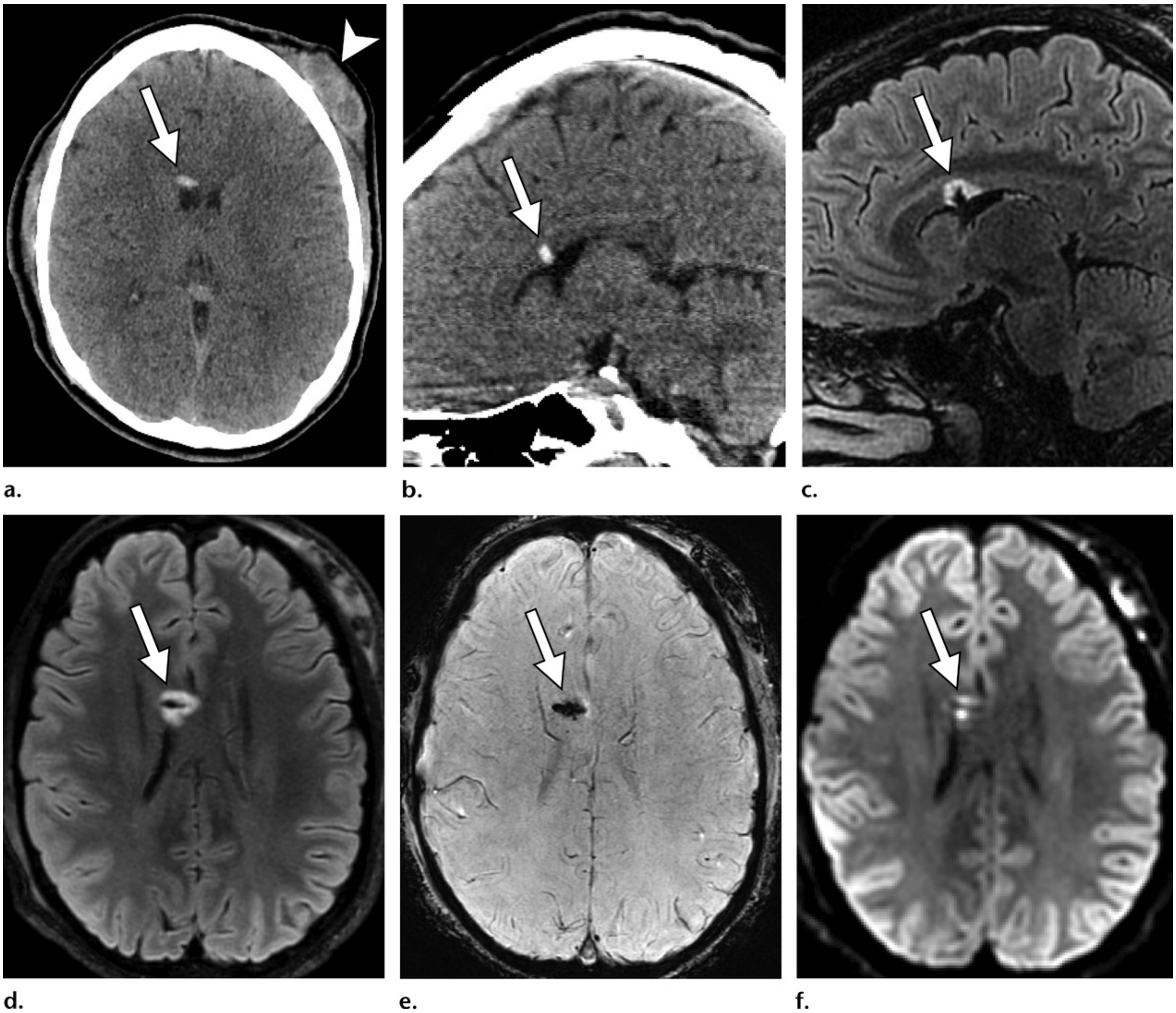

Figure 20. Isolated callosal hemorrhagic axonal injury in a 24-year-old-woman who was struck by a bicycler while jogging and fell forward onto her left forehead. Her GCS score was 14. **(a, b)** Axial **(a)** and sagittal **(b)** nonenhanced head CT images show a large left frontal scalp hematoma (arrowhead in **a**), without an associated skull fracture, and a focal linear hemorrhage (arrow) along the right margin of the anterior body of the corpus callosum. **(c–f)** Sagittal **(c)** and axial **(d)** T2-weighted FLAIR, axial susceptibility-weighted **(e)**, and axial diffusion-weighted **(f)** MR images show surrounding edema (arrows in **c**, **d**), linear hemorrhage (arrow in **e**), and marginal restricted diffusion (arrow in **f**) within the corpus callosum. All are findings compatible with a focal acute TAI. No additional intracranial injuries were noted.

degeneration. As MRI hardware and techniques advanced, it was recognized that shear injuries can occur with milder TBI injuries and to a lesser extent. As a result, the term TAI was used to reflect isolated unifocal or mild multifocal shear injuries (ie, three or fewer foci based on the TBI Common Data Elements) (20,66). DAI will be used in this article as it has the broadest historical definition, although the TBI Common Data Elements define DAI as having four or greater foci.

DAI can be hemorrhagic and/or nonhemorrhagic, and both hemorrhagic and nonhemorrhagic lesions are more sensitively detected at MRI (20,66). Acute DAI lesions may restrict diffusion. Characteristic locations for TAI lesions include the gray-white matter junction (especially in the frontal lobes because the axis of rotation of the head is posterior, allowing greater differences in momentum anteriorly), corpus callosum (especially the splenium), internal capsules, and dorsal midbrain and/or pons. DAI is graded in order of increasing severity. Grade 1 involves the subcortical white matter (Fig 19), grade 2 involves the corpus callosum (Fig 20), and grade 3 involves the brainstem (Fig 21) (95). Thalamic lesions, while not part of the grading system, are associated with poor outcome when present (96).

DAI findings depicted on CT images (and even on MR images) are the tip of the iceberg in that they indicate substantial underlying axonal injury. Clinical findings are usually out of proportion to (ie, more severe than) imaging

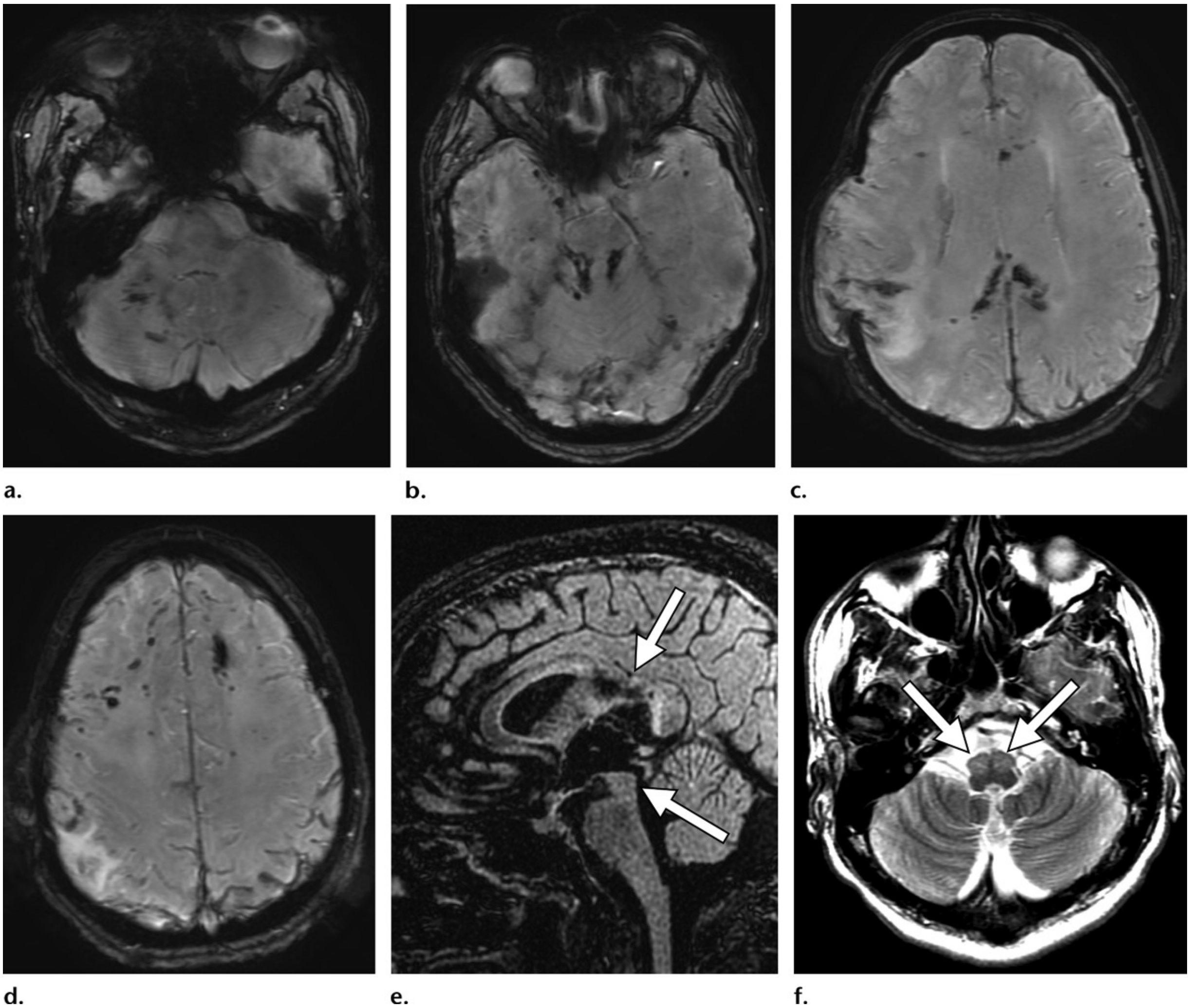

Figure 21. Severe diffuse TAIs in a 25-year-old man following an ATV accident that occurred months earlier, His GCS score was 3. At the time of the accident, the patient underwent an emergent right hemispheric decompressive craniectomy. **(a–d)** Axial susceptibility-weighted MR images show innumerable chronic microhemorrhages throughout the right cerebellar white matter **(a)**, dorsal pons and superior cerebellar peduncles **(b)**, corpus callosum **(c)**, and frontal white matter **(d)**. **(e)** Sagittal T2-weighted FLAIR MR image shows pronounced focal atrophy of the posterior body of the corpus callosum and midbrain (arrows). **(f)** Axial T2-weighted MR image shows bilateral hypertrophic olivary degeneration (arrows), which developed secondary to the severe brainstem TAIs.

findings. DAI usually causes much higher morbidity and mortality than extra-axial injuries and hemorrhagic contusions and is treated with close management of intracranial pressure and craniectomy if necessary to prevent herniation.

Axonal injuries can result in focal T2-hyperintense white matter lesions. However, these lesions are nonspecific and can occur from numerous nontraumatic causes that include ischemic or inflammatory demyelination, chronic migraine headaches, vasculopathies, and other conditions.

A recent prospective multicenter study found that while 27% of young patients (mean age, 23 years) with recent mild TBI had white matter lesions, fewer than 2% were attributable to the acute trauma, and 28% of matched controls also had white matter lesions (97). For patients who underwent imaging with MRI in the acute stage after TBI, unless there is associated diffusion restriction or acute microhemorrhage, white matter T2-hyperintense lesions should be considered nonspecific in cause.

Diffuse Cerebral Edema and Vascular Injuries

Diffuse cerebral edema can result from head injury, possibly due to dysfunctional cerebral autoregulation and blood-brain barrier disruption (98–100). The onset of cerebral edema is variable but is thought to be related to the release of various mediators that can increase blood-brain barrier permeability and result in vasogenic and cytotoxic edema (98,101).

Vascular injuries include arterial dissection (Fig 22) (especially when a fracture traverses the skull base), pseudoaneurysm (most commonly involv-

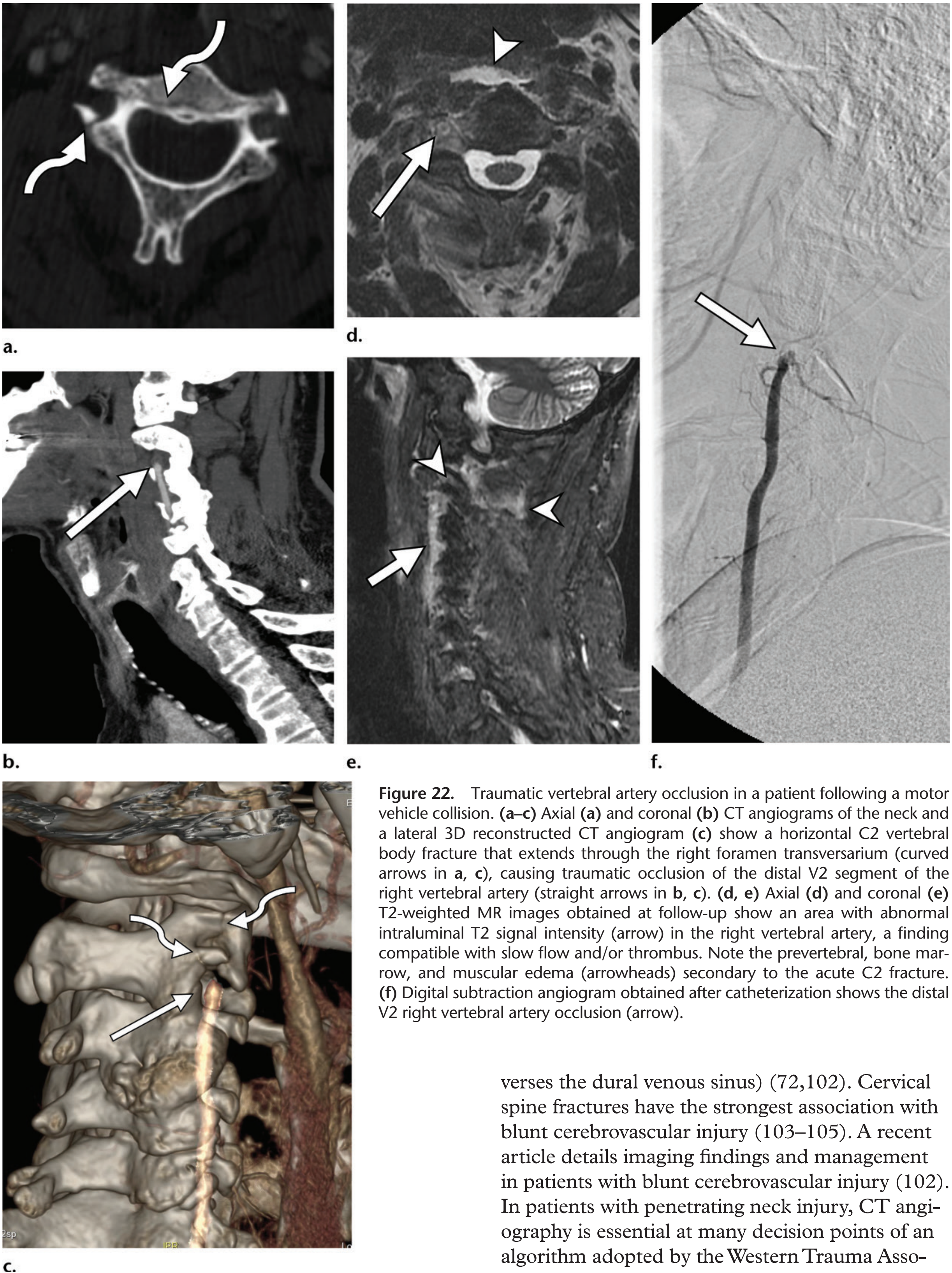

Figure 22. Traumatic vertebral artery occlusion in a patient following a motor vehicle collision. **(a–c)** Axial **(a)** and coronal **(b)** CT angiograms of the neck and a lateral 3D reconstructed CT angiogram **(c)** show a horizontal C2 vertebral body fracture that extends through the right foramen transversarium (curved arrows in **a**, **c**), causing traumatic occlusion of the distal V2 segment of the right vertebral artery (straight arrows in **b**, **c**). **(d, e)** Axial **(d)** and coronal **(e)** T2-weighted MR images obtained at follow-up show an area with abnormal intraluminal T2 signal intensity (arrow) in the right vertebral artery, a finding compatible with slow flow and/or thrombus. Note the prevertebral, bone marrow, and muscular edema (arrowheads) secondary to the acute C2 fracture. **(f)** Digital subtraction angiogram obtained after catheterization shows the distal V2 right vertebral artery occlusion (arrow).

ing the vertebral artery, followed by the anterior cerebral artery), active extravasation, vascular occlusion, traumatic carotid-cavernous fistula (Fig 23), traumatic dural arteriovenous fistula, and venous thrombosis (especially when a fracture traverses the dural venous sinus) (72,102). Cervical spine fractures have the strongest association with blunt cerebrovascular injury (103–105). A recent article details imaging findings and management in patients with blunt cerebrovascular injury (102). In patients with penetrating neck injury, CT angiography is essential at many decision points of an algorithm adopted by the Western Trauma Association, particularly for zone III injuries (superior to the angle of the mandible) (106).

Secondary Brain Injuries and Herniation

Secondary brain injuries are caused by mass effect resulting in herniation, which can lead to infarctions, hydrocephalus, and hemorrhages (107).

Figure 23. Traumatic direct carotid-cavernous fistula in a 50-year-old man with alcoholism who was found unconscious on the sidewalk. **(a)** Coronal nonenhanced CT image shows multiple maxillofacial fractures, including the right orbit (straight arrow) and left orbital roof and sphenoid bone (curved arrows). **(b)** Follow-up axial MR angiogram shows pronounced arterialized flow-related enhancement in the cavernous sinuses (arrowheads), left ophthalmic vein, and sphenoparietal sinus (arrows). **(c)** Coronal T2-weighted MR image shows diffuse intraorbital edema (arrowheads) and small bilateral subdural hygromas (arrows). **(d)** Axial T1-weighted MR image shows the ophthalmic veins (arrows) markedly dilated and a small subacute hemorrhagic contusion (arrowhead). **(e)** Axial gadolinium-enhanced T1-weighted MR image shows asymmetric left ocular proptosis (arrows). These findings are compatible with occult high-flow direct carotid-cavernous fistula. **(f, g)** Digital subtraction angiograms obtained after catheterization show direct arterial flow from the left cavernous carotid artery into the left cavernous sinus (straight arrow), also filling the contralateral right cavernous sinus through intersellar communications. Note the arterialized flow within the left ophthalmic vein (arrowhead) and left sphenoparietal sinus (curved arrow).

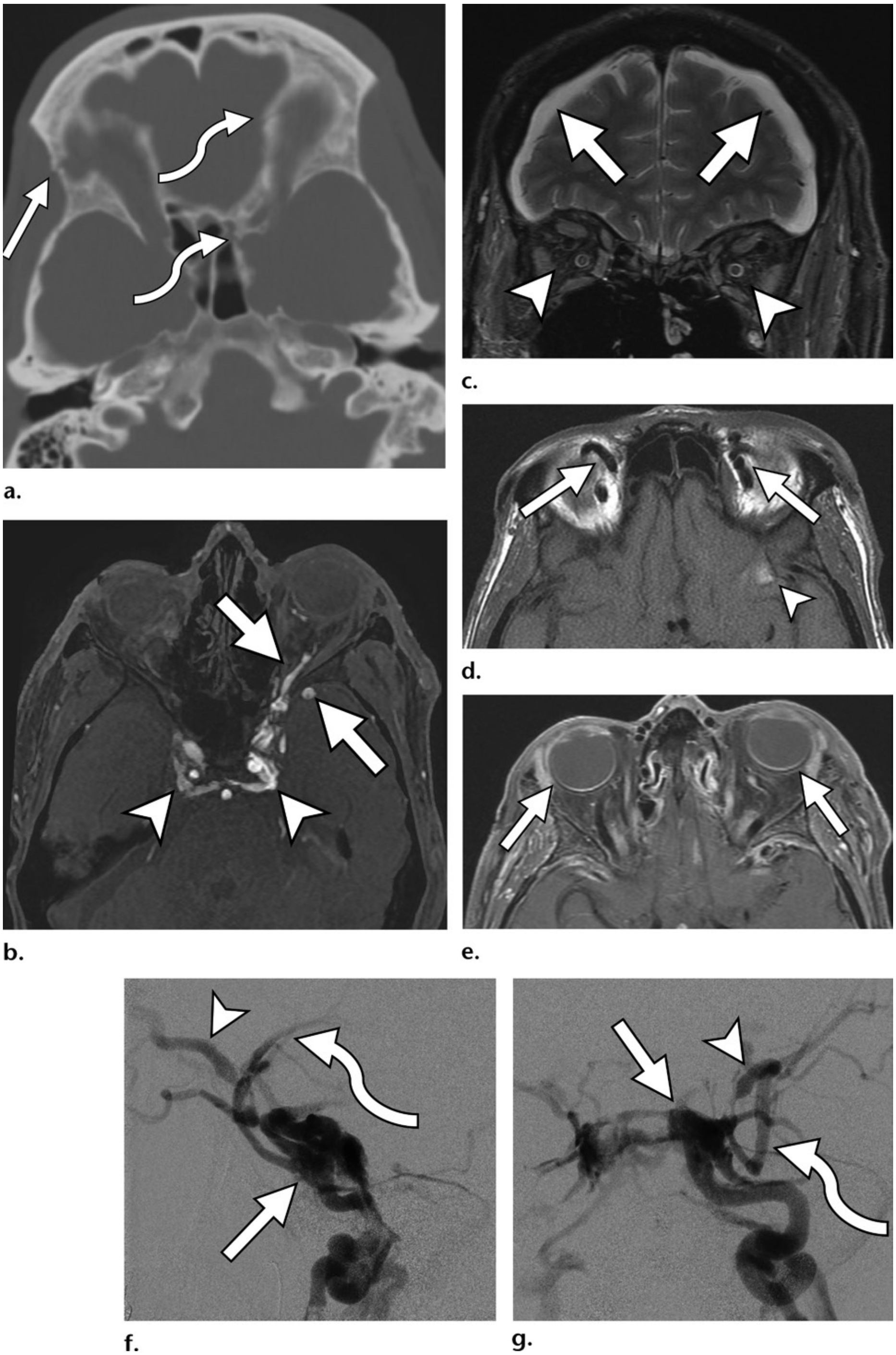

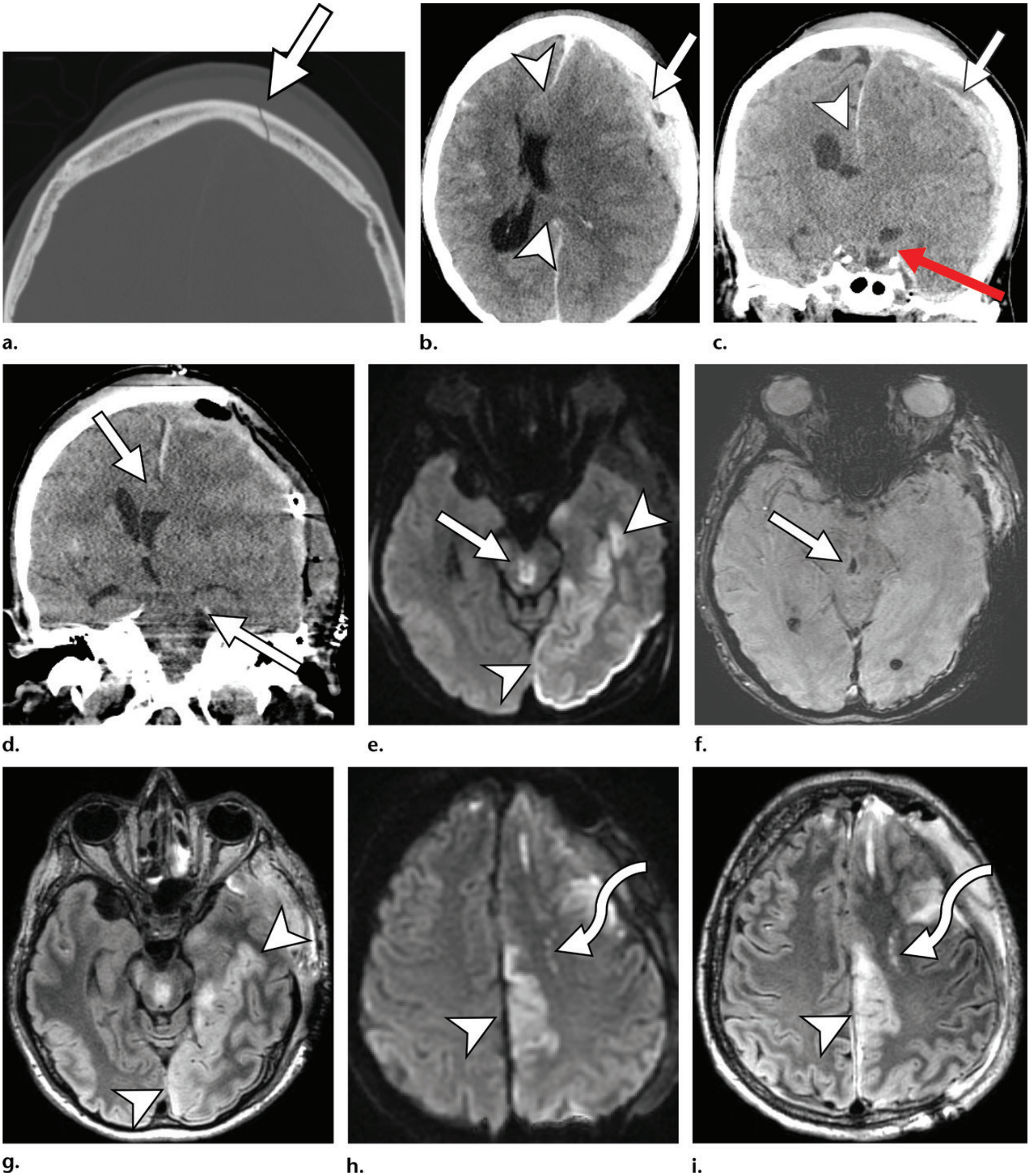

Figure 24. Secondary cerebral infarctions in a 34-year-old man who fell from scaffolding and was unconscious. His GCS score was 4. **(a)** Axial nonenhanced CT image shows a nondisplaced left frontal calvarial fracture (arrow). **(b, c)** Axial **(b)** and coronal **(c)** nonenhanced CT images show a large mixed-attenuating hyperacute and acute left cerebral convexity hematoma (white arrow) causing mass effect, rightward subfalcine herniation (arrowheads), and central downward herniation with effacement of the suprasellar cistern with brainstem compression (red arrow in **c**). **(d)** Coronal nonenhanced CT image shows improved right subfalcine and central downward herniation (arrows) after emergency decompressive craniectomy. **(e, f)** Axial diffusion-weighted image **(e)** shows central midbrain infarction (arrow in **e**), with associated hemorrhage (arrow in **f**) on the axial susceptibility-weighted image **(f)**. **(g)** Axial T2-weighted FLAIR MR image shows a large left anterior cerebral artery infarction (arrowheads in **e**, **g**). **(h, i)** Axial diffusion-weighted **(h)** and T2-weighted FLAIR **(i)** MR images show a distal left anterior cerebral artery (arrowheads) related to vascular compression from herniation and multifocal T2-hyperintense restricted foci (curved arrow), compatible with TAIs. Diffuse SAH, intraventricular hemorrhage, and multifocal frontal contusions were also noted.

Downward transtentorial herniation can result in third nerve palsy with pupillary involvement ("blown" mydriatic pupil). Various types of herniation can also result in secondary cerebral infarctions (108,109) (Fig 24): *(a)* subfalcine herniation can cause anterior cerebral artery infarction on the side of the mass effect owing to compression of the anterior cerebral artery against the falx; *(b)* unilateral or

Potential Complications Due to Herniation in the Setting of TBI

Type of Herniation	Ischemic Complications	Ventricular Entrapment and Other Findings
Subfalcine herniation (midline shift)	Anterior cerebral artery infarction on the side of the mass effect	Lateral ventriculomegaly on the side that the midline is shifting toward
Unilateral or asymmetric downward transtentorial herniation	Ipsilateral posterior cerebral artery infarction	Ipsilateral cranial nerve III palsy with pupillary involvement; ipsilateral hemiparesis (Kernohan phenomenon, if severe)
Severe or bilateral downward transtentorial herniation	Circle of Willis perforator occlusion; hypothalamic and basal ganglia infarctions	Midbrain Duret hemorrhages
Ascending transtentorial herniation	Superior cerebellar artery infarction (if severe)	Noncommunicating hydrocephalus at the level of the cerebral aqueduct
Cerebellar tonsillar herniation	Posterior inferior cerebellar artery infarction (if severe)	Noncommunicating hydrocephalus at the fourth ventricular outlet

asymmetric downward transtentorial herniation can result in ipsilateral posterior cerebral artery infarction; *(c)* severe bilateral downward transtentorial herniation can compress perforating arteries arising from the circle of Willis, resulting in hypothalamic and basal ganglia infarctions; and *(d)* severe cerebellar tonsillar herniation can result in posterior inferior cerebellar artery infarction.

Various herniation patterns can also result in ventricular entrapment (Fig 24): *(a)* subfalcine herniation can occlude the foramen of Monro and result in lateral ventriculomegaly; *(b)* ascending transtentorial herniation effaces the quadrigeminal plate cistern, compresses the midbrain, and can result in noncommunicating hydrocephalus at the level of the cerebral aqueduct; and *(c)* cerebellar tonsillar herniation can cause fourth ventricular outlet obstruction and resulting hydrocephalus. Secondary midbrain (Duret) hemorrhages (Figs 5, 24) occur in severe downward transtentorial herniation. These complications are summarized in the Table.

Conclusion

Radiologists play a critical role in the diagnosis of complications of TBI and should understand injury patterns based on mechanism of injury, as well as secondary injuries that can occur owing to mass effect and herniation. CT is most important in acute TBI given its speed, accessibility, and high sensitivity for detecting lesions requiring neurosurgical intervention. MRI has higher sensitivity for the detection of intracranial injuries; while its optimal use in TBI is an area of active investigation, MRI is currently indicated when CT is normal and there are persistent unexplained neurologic findings. DTI remains investigational for assessment of TBI in patients.

***Disclosures of Conflicts of Interest.*—S.N.N.** *Activities related to the present article:* grant from the ACR to develop TBI-RADS. *Activities not related to the present article:* disclosed no relevant relationships. *Other activities:* disclosed no relevant relationships. **A.J.T.** *Activities related to the present article:* disclosed no relevant relationships. *Activities not related to the present article:* blinded structured expert readings for clinical trails for BioClinica, Parexel, and ICON; expert medicolegal testimony for medical negligence and personal injury litigation, primarily for TBI that involves DTI. *Other activities:* disclosed no relevant relationships.

References

1. Dewan MC, Rattani A, Gupta S, et al. Estimating the global incidence of traumatic brain injury. J Neurosurg 2018:1–18 [Epub ahead of print] https://doi.org/10.3171/2017.10.JNS17352.
2. GBD 2016 Traumatic Brain Injury and Spinal Cord Injury Collaborators. Global, regional, and national burden of traumatic brain injury and spinal cord injury, 1990-2016: a systematic analysis for the Global Burden of Disease Study 2016. Lancet Neurol 2019;18(1):56–87.
3. Taylor CA, Bell JM, Breiding MJ, Xu L. Traumatic Brain Injury-Related Emergency Department Visits, Hospitalizations, and Deaths - United States, 2007 and 2013. MMWR Surveill Summ 2017;66(9):1–16.
4. Wintermark M, Sanelli PC, Anzai Y, et al. Imaging evidence and recommendations for traumatic brain injury: conventional neuroimaging techniques. J Am Coll Radiol 2015;12(2):e1–e14.
5. Teasdale G, Maas A, Lecky F, Manley G, Stocchetti N, Murray G. The Glasgow Coma Scale at 40 years: standing the test of time. Lancet Neurol 2014;13(8):844–854.
6. Brown JB, Forsythe RM, Stassen NA, et al. Evidence-based improvement of the National Trauma Triage Protocol: The Glasgow Coma Scale versus Glasgow Coma Scale motor subscale. J Trauma Acute Care Surg 2014;77(1):95–102; discussion 101–102.
7. Chou R, Totten AM, Pappas M, et al. Glasgow Coma Scale for Field Triage of Trauma: A Systematic Review. Rockville, Md: Agency for Healthcare Research and Quality, 2017.
8. Sussman ES, Pendharkar AV, Ho AL, Ghajar J. Mild traumatic brain injury and concussion: terminology and classification. Handb Clin Neurol 2018;158:21–24.
9. Management of Concussion/mTBI Working Group. VA/DoD Clinical Practice Guideline for Management of Concussion/Mild Traumatic Brain Injury. J Rehabil Res Dev 2009;46(6):CP1–CP68.
10. Giza CC, Kutcher JS, Ashwal S, et al. Summary of evidence-based guideline update: evaluation and management of concussion in sports—report of the Guideline Development

Subcommittee of the American Academy of Neurology. Neurology 2013;80(24):2250–2257.

11. Shetty VS, Reis MN, Aulino JM, et al. ACR Appropriateness Criteria Head Trauma. J Am Coll Radiol. 2016 Jun;13(6):668-79.
12. Haydel MJ, Preston CA, Mills TJ, Luber S, Blaudeau E, DeBlieux PM. Indications for computed tomography in patients with minor head injury. N Engl J Med 2000;343(2):100–105.
13. Stiell IG, Wells GA, Vandemheen K, et al. The Canadian CT Head Rule for patients with minor head injury. Lancet 2001;357(9266):1391–1396.
14. Mower WR, Hoffman JR, Herbert M, et al. Developing a decision instrument to guide computed tomographic imaging of blunt head injury patients. J Trauma 2005;59(4):954–959.
15. Wei SC, Ulmer S, Lev MH, Pomerantz SR, González RG, Henson JW. Value of coronal reformations in the CT evaluation of acute head trauma. AJNR Am J Neuroradiol 2010;31(2):334–339.
16. Añon J, Remonda L, Spreng A, et al. Traumatic extra-axial hemorrhage: correlation of postmortem MSCT, MRI, and forensic-pathological findings. J Magn Reson Imaging 2008;28(4):823–836.
17. Gentry LR, Godersky JC, Thompson B, Dunn VD. Prospective comparative study of intermediate-field MR and CT in the evaluation of closed head trauma. AJR Am J Roentgenol 1988;150(3):673–682.
18. Han JS, Kaufman B, Alfidi RJ, et al. Head trauma evaluated by magnetic resonance and computed tomography: a comparison. Radiology 1984;150(1):71–77.
19. Kelly AB, Zimmerman RD, Snow RB, Gandy SE, Heier LA, Deck MD. Head trauma: comparison of MR and CT—experience in 100 patients. AJNR Am J Neuroradiol 1988;9(4):699–708.
20. Paterakis K, Karantanas AH, Komnos A, Volikas Z. Outcome of patients with diffuse axonal injury: the significance and prognostic value of MRI in the acute phase. J Trauma 2000;49(6):1071–1075.
21. Snow RB, Zimmerman RD, Gandy SE, Deck MD. Comparison of magnetic resonance imaging and computed tomography in the evaluation of head injury. Neurosurgery 1986;18(1):45–52.
22. Zimmerman RA, Bilaniuk LT, Hackney DB, Goldberg HI, Grossman RI. Head injury: early results of comparing CT and high-field MR. AJR Am J Roentgenol 1986;147(6):1215–1222.
23. Mitchell P, Wilkinson ID, Hoggard N, et al. Detection of subarachnoid haemorrhage with magnetic resonance imaging. J Neurol Neurosurg Psychiatry 2001;70(2):205–211.
24. Hesselink JR, Dowd CF, Healy ME, Hajek P, Baker LL, Luerssen TG. MR imaging of brain contusions: a comparative study with CT. AJR Am J Roentgenol 1988;150(5):1133–1142.
25. Noguchi K, Seto H, Kamisaki Y, Tomizawa G, Toyoshima S, Watanabe N. Comparison of fluid-attenuated inversion-recovery MR imaging with CT in a simulated model of acute subarachnoid hemorrhage. AJNR Am J Neuroradiol 2000;21(5):923–927.
26. Noguchi K, Ogawa T, Seto H, et al. Subacute and chronic subarachnoid hemorrhage: diagnosis with fluid-attenuated inversion-recovery MR imaging. Radiology 1997;203(1):257–262.
27. Woodcock RJ Jr, Short J, Do HM, Jensen ME, Kallmes DF. Imaging of acute subarachnoid hemorrhage with a fluid-attenuated inversion recovery sequence in an animal model: comparison with non-contrast-enhanced CT. AJNR Am J Neuroradiol 2001;22(9):1698–1703.
28. Kara A, Celik SE, Dalbayrak S, Yilmaz M, Akansel G, Tireli G. Magnetic resonance imaging finding in severe head injury patients with normal computerized tomography. Turk Neurosurg 2008;18(1):1–9.
29. Greenberg SM, Vernooij MW, Cordonnier C, et al. Cerebral microbleeds: a guide to detection and interpretation. Lancet Neurol 2009;8(2):165–174.
30. Beauchamp MH, Ditchfield M, Babl FE, et al. Detecting traumatic brain lesions in children: CT versus MRI versus susceptibility weighted imaging (SWI). J Neurotrauma 2011;28(6):915–927.
31. Geurts BHJ, Andriessen TMJC, Goraj BM, Vos PE. The reliability of magnetic resonance imaging in traumatic brain injury lesion detection. Brain Inj 2012;26(12):1439–1450.
32. Huang YL, Kuo YS, Tseng YC, Chen DYT, Chiu WT, Chen CJ. Susceptibility-weighted MRI in mild traumatic brain injury. Neurology 2015;84(6):580–585.
33. Trifan G, Gattu R, Haacke EM, Kou Z, Benson RR. MR imaging findings in mild traumatic brain injury with persistent neurological impairment. Magn Reson Imaging 2017;37:243–251.
34. Liu AY, Maldjian JA, Bagley LJ, Sinson GP, Grossman RI. Traumatic brain injury: diffusion-weighted MR imaging findings. AJNR Am J Neuroradiol 1999;20(9):1636–1641.
35. Hergan K, Schaefer PW, Sorensen AG, Gonzalez RG, Huisman TA. Diffusion-weighted MRI in diffuse axonal injury of the brain. Eur Radiol 2002;12(10):2536–2541.
36. Ezaki Y, Tsutsumi K, Morikawa M, Nagata I. Role of diffusion-weighted magnetic resonance imaging in diffuse axonal injury. Acta Radiol 2006;47(7):733–740.
37. Roth TL, Nayak D, Atanasijevic T, Koretsky AP, Latour LL, McGavern DB. Transcranial amelioration of inflammation and cell death after brain injury. Nature 2014;505(7482):223–228.
38. Kim SC, Park SW, Ryoo I, et al. Contrast-enhanced FLAIR (fluid-attenuated inversion recovery) for evaluating mild traumatic brain injury. PLoS One 2014;9(7):e102229.
39. Chiara Ricciardi M, Bokkers RPH, Butman JA, et al. Trauma-Specific Brain Abnormalities in Suspected Mild Traumatic Brain Injury Patients Identified in the First 48 Hours after Injury: A Blinded Magnetic Resonance Imaging Comparative Study Including Suspected Acute Minor Stroke Patients. J Neurotrauma 2017;34(1):23–30.
40. Bodanapally UK, Saksobhavivat N, Shanmuganathan K, Aarabi B, Roy AK. Arterial injuries after penetrating brain injury in civilians: risk factors on admission head computed tomography. J Neurosurg 2015;122(1):219–226.
41. Perrein A, Petry L, Reis A, Baumann A, Mertes P, Audibert G. Cerebral vasospasm after traumatic brain injury: an update. Minerva Anestesiol 2015;81(11):1219–1228.
42. Expert Panel on Neurologic Imaging. Salmela MB, Mortazavi S, et al. ACR Appropriateness Criteria® Cerebrovascular Disease. J Am Coll Radiol 2017;14(5S):S34–S61.
43. Rischall MA, Boegel KH, Palmer CS, Knoll B, McKinney AM. MDCT Venographic Patterns of Dural Venous Sinus Compromise After Acute Skull Fracture. AJR Am J Roentgenol 2016;207(4):852–858.
44. Fujii Y, Tasaki O, Yoshiya K, et al. Evaluation of posttraumatic venous sinus occlusion with CT venography. J Trauma 2009;66(4):1002–1006; discussion 1006–1007.
45. Delgado Almandoz JE, Kelly HR, Schaefer PW, Lev MH, Gonzalez RG, Romero JM. Prevalence of traumatic dural venous sinus thrombosis in high-risk acute blunt head trauma patients evaluated with multidetector CT venography. Radiology 2010;255(2):570–577.
46. Rivkin MA, Saraiya PV, Woodrow SI. Sinovenous thrombosis associated with skull fracture in the setting of blunt head trauma. Acta Neurochir (Wien) 2014;156(5):999–1007; discussion 1007.
47. Slasky SE, Rivaud Y, Suberlak M, et al. Venous Sinus Thrombosis in Blunt Trauma: Incidence and Risk Factors. J Comput Assist Tomogr 2017;41(6):891–897.
48. Niogi SN, Mukherjee P. Diffusion tensor imaging of mild traumatic brain injury. J Head Trauma Rehabil 2010;25(4):241–255.
49. Xiong Y, Zhou XJ, Nisi RA, et al. Brain white matter changes in CPAP-treated obstructive sleep apnea patients with residual sleepiness. J Magn Reson Imaging 2017;45(5):1371–1378.
50. Xie Y, Zhang Y, Qin W, Lu S, Ni C, Zhang Q. White Matter Microstructural Abnormalities in Type 2 Diabetes Mellitus: A Diffusional Kurtosis Imaging Analysis. AJNR Am J Neuroradiol 2017;38(3):617–625.
51. Li X, Ma C, Sun X, et al. Disrupted white matter structure underlies cognitive deficit in hypertensive patients. Eur Radiol 2016;26(9):2899–2907.
52. Abe O, Aoki S, Hayashi N, et al. Normal aging in the central nervous system: quantitative MR diffusion-tensor analysis. Neurobiol Aging 2002;23(3):433–441.

53. Bender AR, Völkle MC, Raz N. Differential aging of cerebral white matter in middle-aged and older adults: A seven-year follow-up. Neuroimage 2016;125:74–83.
54. Ohtani T, Nestor PG, Bouix S, et al. Exploring the neural substrates of attentional control and human intelligence: Diffusion tensor imaging of prefrontal white matter tractography in healthy cognition. Neuroscience 2017;341:52–60.
55. Niogi S, Mukherjee P, Ghajar J, McCandliss BD. Individual Differences in Distinct Components of Attention are Linked to Anatomical Variations in Distinct White Matter Tracts. Front Neuroanat 2010;4:2.
56. Johnson NF, Kim C, Gold BT. Socioeconomic status is positively correlated with frontal white matter integrity in aging. Age (Dordr) 2013;35(6):2045–2056.
57. Stokum JA, Sours C, Zhuo J, Kane R, Shanmuganathan K, Gullapalli RP. A longitudinal evaluation of diffusion kurtosis imaging in patients with mild traumatic brain injury. Brain Inj 2015;29(1):47–57.
58. Lemkaddem A, Daducci A, Vulliemoz S, et al. A multicenter study: intra-scan and inter-scan variability of diffusion spectrum imaging. Neuroimage 2012;62(1):87–94.
59. White NS, Leergaard TB, D'Arceuil H, Bjaalie JG, Dale AM. Probing tissue microstructure with restriction spectrum imaging: Histological and theoretical validation. Hum Brain Mapp 2013;34(2):327–346.
60. Zhang H, Schneider T, Wheeler-Kingshott CA, Alexander DC. NODDI: practical in vivo neurite orientation dispersion and density imaging of the human brain. Neuroimage 2012;61(4):1000–1016.
61. Maas AIR, Hukkelhoven CWPM, Marshall LF, Steyerberg EW. Prediction of outcome in traumatic brain injury with computed tomographic characteristics: a comparison between the computed tomographic classification and combinations of computed tomographic predictors. Neurosurgery 2005;57(6):1173–1182; discussion 1173–1182.
62. Mata-Mbemba D, Mugikura S, Nakagawa A, et al. Early CT findings to predict early death in patients with traumatic brain injury: Marshall and Rotterdam CT scoring systems compared in the major academic tertiary care hospital in northeastern Japan. Acad Radiol 2014;21(5):605–611.
63. Wintermark M, Li Y, Ding VY, et al. Neuroimaging Radiological Interpretation System for Acute Traumatic Brain Injury. J Neurotrauma 2018;35(22):2665–2672.
64. Marincowitz C, Lecky FE, Townend W, Borakati A, Fabbri A, Sheldon TA. The Risk of Deterioration in GCS13-15 Patients with Traumatic Brain Injury Identified by Computed Tomography Imaging: A Systematic Review and Meta-Analysis. J Neurotrauma 2018;35(5):703–718.
65. Yuh EL, Cooper SR, Ferguson AR, Manley GT. Quantitative CT improves outcome prediction in acute traumatic brain injury. J Neurotrauma 2012;29(5):735–746.
66. Yuh EL, Mukherjee P, Lingsma HF, et al. Magnetic resonance imaging improves 3-month outcome prediction in mild traumatic brain injury. Ann Neurol 2013;73(2):224–235.
67. Cicuendez M, Castaño-León A, Ramos A, Hilario A, Gómez PA, Lagares A. The added prognostic value of magnetic resonance imaging in traumatic brain injury: The importance of traumatic axonal injury when performing ordinal logistic regression. J Neuroradiol 2018 Sep 1 [Epub ahead of print].
68. Haghbayan H, Boutin A, Laflamme M, et al. The Prognostic Value of MRI in Moderate and Severe Traumatic Brain Injury: A Systematic Review and Meta-Analysis. Crit Care Med 2017;45(12):e1280–e1288.
69. ACR Head Injury Institute. TBI-RADS. http://www.headinjuryinstitute.org/tools/hi-rads/. Accessed March 22, 2019.
70. Cramer JA, Eisenmenger LB, Pierson NS, Dhatt HS, Heilbrun ME. Structured and templated reporting: An overview. Appl Radiol 2014. https://appliedradiology.com/articles/structured-and-templated-reporting-an-overview. Accessed March 22, 2019.
71. Allen B, Chatfield M, Burleson J, Thorwarth WT. Improving diagnosis in health care: perspectives from the American College of Radiology. Diagnosis (Berl) 2017;4(3):113–124.
72. Baugnon KL, Hudgins PA. Skull base fractures and their complications. Neuroimaging Clin N Am 2014;24(3):439–465, vii–viii.
73. Zayas JO, Feliciano YZ, Hadley CR, Gomez AA, Vidal JA. Temporal bone trauma and the role of multidetector CT in the emergency department. RadioGraphics 2011;31(6):1741–1755.
74. Ellis H. Anatomy of head injury. Surgery 2012;30(3):99–101.
75. Al-Nakshabandi NA. The swirl sign. Radiology 2001;218(2):433.
76. Gean AD, Fischbein NJ, Purcell DD, Aiken AH, Manley GT, Stiver SI. Benign anterior temporal epidural hematoma: indolent lesion with a characteristic CT imaging appearance after blunt head trauma. Radiology 2010;257(1):212–218.
77. Peres CMA, Caldas JGMP, Puglia P, et al. Endovascular management of acute epidural hematomas: clinical experience with 80 cases. J Neurosurg 2018;128(4):1044–1050.
78. Sieswerda-Hoogendoorn T, Postema FAM, Verbaan D, Majoie CB, van Rijn RR. Age determination of subdural hematomas with CT and MRI: a systematic review. Eur J Radiol 2014;83(7):1257–1268.
79. Ban SP, Hwang G, Byoun HS, et al. Middle Meningeal Artery Embolization for Chronic Subdural Hematoma. Radiology 2018;286(3):992–999.
80. Link TW, Boddu S, Paine SM, Kamel H, Knopman J. Middle Meningeal Artery Embolization for Chronic Subdural Hematoma: A Series of 60 Cases. Neurosurgery 2018 Nov 9 [Epub ahead of print] https://doi.org/10.1093/neuros/nyy521.
81. Zanini MA, de Lima Resende LA, de Souza Faleiros AT, Gabarra RC. Traumatic subdural hygromas: proposed pathogenesis based classification. J Trauma 2008;64(3):705–713.
82. Bodanapally UK, Dreizin D, Issa G, Archer-Arroyo KL, Sudini K, Fleiter TR. Dual-Energy CT in Enhancing Subdural Effusions that Masquerade as Subdural Hematomas: Diagnosis with Virtual High-Monochromatic (190-keV) Images. AJNR Am J Neuroradiol 2017;38(10):1946–1952.
83. Zouros A, Bhargava R, Hoskinson M, Aronyk KE. Further characterization of traumatic subdural collections of infancy. Report of five cases. J Neurosurg 2004;100(5 Suppl Pediatrics):512–518.
84. Vezina G. Assessment of the nature and age of subdural collections in nonaccidental head injury with CT and MRI. Pediatr Radiol 2009;39(6):586–590.
85. Borczuk P, Penn J, Peak D, Chang Y. Patients with traumatic subarachnoid hemorrhage are at low risk for deterioration or neurosurgical intervention. J Trauma Acute Care Surg 2013;74(6):1504–1509.
86. Servadei F, Murray GD, Teasdale GM, et al. Traumatic subarachnoid hemorrhage: demographic and clinical study of 750 patients from the European brain injury consortium survey of head injuries. Neurosurgery 2002;50(2):261–267; discussion 267–269.
87. Mata-Mbemba D, Mugikura S, Nakagawa A, et al. Traumatic midline subarachnoid hemorrhage on initial computed tomography as a marker of severe diffuse axonal injury. J Neurosurg 2018;129(5):1317–1324.
88. Takenaka N, Mine T, Suga S, et al. Interpeduncular high-density spot in severe shearing injury. Surg Neurol 1990;34(1):30–38.
89. Mata-Mbemba D, Mugikura S, Nakagawa A, et al. Intraventricular hemorrhage on initial computed tomography as marker of diffuse axonal injury after traumatic brain injury. J Neurotrauma 2015;32(5):359–365.
90. Yue JK, Winkler EA, Puffer RC, et al. Temporal lobe contusions on computed tomography are associated with impaired 6-month functional recovery after mild traumatic brain injury: a TRACK-TBI study. Neurol Res 2018;40(11):972–981.
91. Scheid R, Ott DV, Roth H, Schroeter ML, von Cramon DY. Comparative magnetic resonance imaging at 1.5 and 3 Tesla for the evaluation of traumatic microbleeds. J Neurotrauma 2007;24(12):1811–1816.
92. Alahmadi H, Vachhrajani S, Cusimano MD. The natural history of brain contusion: an analysis of radiological and clinical progression. J Neurosurg 2010;112(5):1139–1145.
93. Chieregato A, Fainardi E, Morselli-Labate AM, et al. Factors associated with neurological outcome and lesion progression in traumatic subarachnoid hemorrhage patients. Neurosurgery 2005;56(4):671–680; discussion 671–680.

94. Saeki N, Yamaura A, Sunami K. Brain stem contusion due to tentorial coup injury: case report and pathomechanical analysis from normal cadavers. Br J Neurosurg 1998;12(2):151–155.
95. Adams JH, Doyle D, Ford I, Gennarelli TA, Graham DI, McLellan DR. Diffuse axonal injury in head injury: definition, diagnosis and grading. Histopathology 1989;15(1):49–59.
96. Moen KG, Brezova V, Skandsen T, Håberg AK, Folvik M, Vik A. Traumatic axonal injury: the prognostic value of lesion load in corpus callosum, brain stem, and thalamus in different magnetic resonance imaging sequences. J Neurotrauma 2014;31(17):1486–1496.
97. Shetty T, Nguyen JT, Cogsil T, et al. Clinical Findings in a Multicenter MRI Study of Mild TBI. Front Neurol 2018;9:836.
98. Unterberg AW, Stover J, Kress B, Kiening KL. Edema and brain trauma. Neuroscience 2004;129(4):1021–1029.
99. Golding EM. Sequelae following traumatic brain injury. The cerebrovascular perspective. Brain Res Brain Res Rev 2002;38(3):377–388.
100. Werner C, Engelhard K. Pathophysiology of traumatic brain injury. Br J Anaesth 2007;99(1):4–9.
101. Marmarou A, Signoretti S, Fatouros PP, Portella G, Aygok GA, Bullock MR. Predominance of cellular edema in traumatic brain swelling in patients with severe head injuries. J Neurosurg 2006;104(5):720–730.
102. Rutman AM, Vranic JE, Mossa-Basha M. Imaging and Management of Blunt Cerebrovascular Injury. RadioGraphics 2018;38(2):542–563.
103. Biffl WL, Moore EE, Offner PJ, et al. Optimizing screening for blunt cerebrovascular injuries. Am J Surg 1999;178(6):517–522.
104. Franz RW, Willette PA, Wood MJ, Wright ML, Hartman JF. A systematic review and meta-analysis of diagnostic screening criteria for blunt cerebrovascular injuries. J Am Coll Surg 2012;214(3):313–327.
105. Cothren CC, Moore EE, Biffl WL, et al. Cervical spine fracture patterns predictive of blunt vertebral artery injury. J Trauma 2003;55(5):811–813.
106. Sperry JL, Moore EE, Coimbra R, et al. Western Trauma Association critical decisions in trauma: penetrating neck trauma. J Trauma Acute Care Surg 2013;75(6):936–940.
107. Johnson PL, Eckard DA, Chason DP, Brecheisen MA, Batnitzky S. Imaging of acquired cerebral herniations. Neuroimaging Clin N Am 2002;12(2):217–228.
108. Tawil I, Stein DM, Mirvis SE, Scalea TM. Posttraumatic cerebral infarction: incidence, outcome, and risk factors. J Trauma 2008;64(4):849–853.
109. Bae DH, Choi KS, Yi HJ, Chun HJ, Ko Y, Bak KH. Cerebral Infarction after Traumatic Brain Injury: Incidence and Risk Factors. Korean J Neurotrauma 2014;10(2):35–40.

This journal-based SA-CME activity has been approved for ***AMA PRA Category 1 Credit™*****.** *See rsna.org/learning-center-rg.*